Methoden moderner Röntgenphysik II: Streuung und Abbildung

Vorlesung zum Haupt- oder Masterstudiengang Physik, SoSe 2019

G. Grübel, F. Lehmkühler, L. Müller, O. Seeck

Location Lecture hall INF, Physics, Jungiusstraße 11

Time Tuesday 12:30 - 14:30
Thursday 8:30 - 10:00

DESY

Outline

Part II/3:

Studies on Magnetic Nanostructures

by Leonard Müller

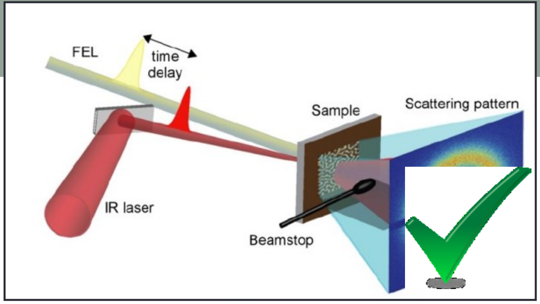

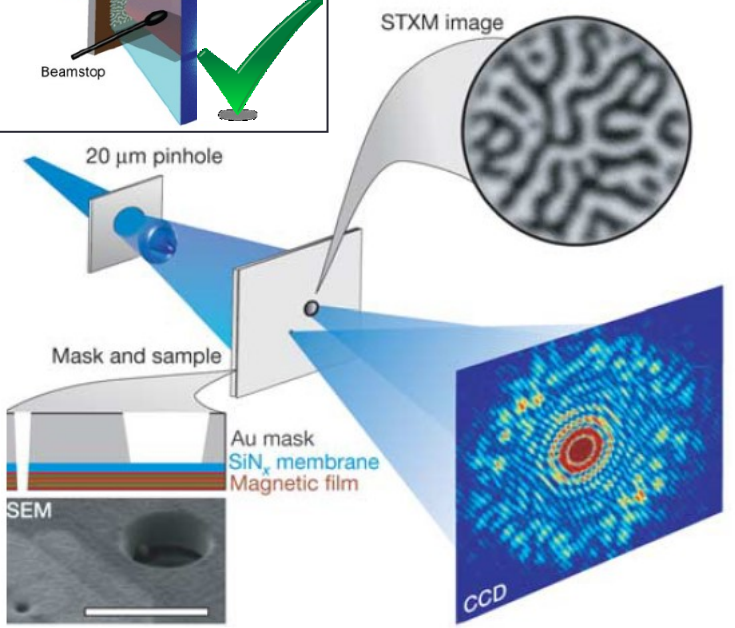

[18.6.] Imaging of Magnetic Domains

- **(Hard) X-ray imaging (, small selection of)**
- **Fourier Transform Holography (FTH)**
- Scanning Transmission X-ray Microscopy (STXM)
- Coherent Diffraction Imaging (CDI)

Lensless imaging of magnetic nanostructures by X-ray spectro-holography

S. Eisebitt[1], J. Lüning[2], W. F. Schlotter[2,3], M. Lörgen[1], O. Hellwig[1,4], W. Eberhardt[1] & J. Stöhr[2]

NATURE | VOL 432 | 16 DECEMBER 2004 |

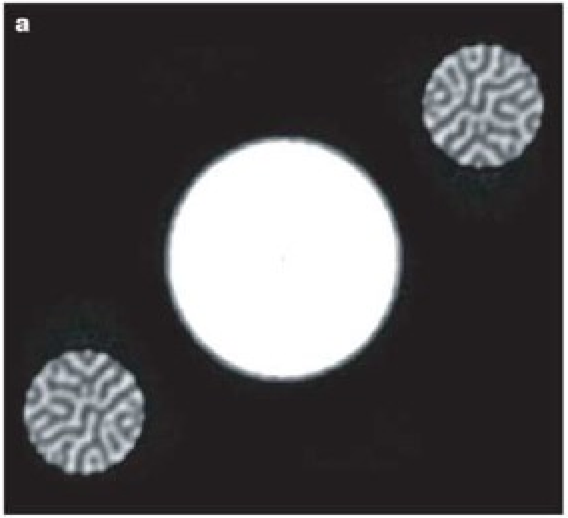

FTH

Exkursion zu DESY am 25.6.

Beginn: 13:00

Treffpunkt: PR Point in Gebäude 48f – Ada Yonath Halle (Petra III extension)

Inhalte: DESY FS, Petra III Halle, FLASH Halle, Liquid Jet Labor

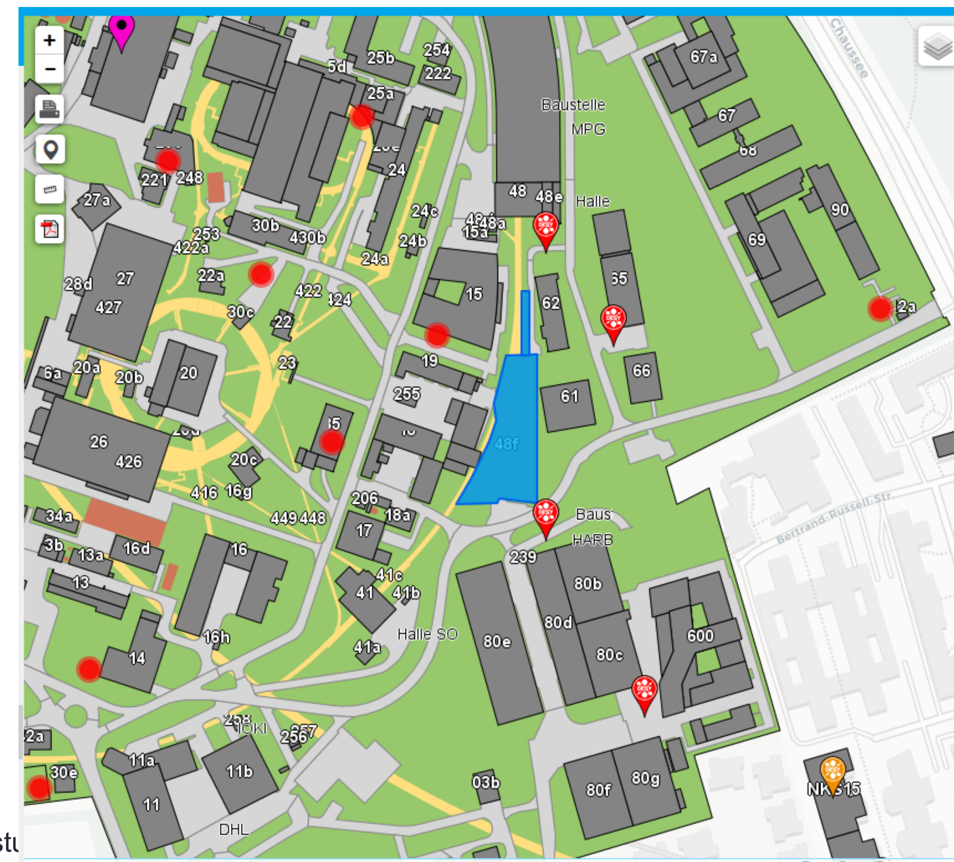

- Part I

Hard X-ray imaging

The university Göttingen team and collaborators

Matthias Bartels *waveguide holography, tomography, neural cells and tissues*
Robin Wilke, *phase reconstruction algorithms, ptychography*
Martin Krenkel *phase reconstruction*
Klaus Giewekemeier *phase reconstruction algorithms, ptychography, cellular imaging* (now at eXFEL)

Sebastian Aeffner *membrane fusion intermediates* (now Univ. Würzburg)
Simon Castorph synaptic vesicles (now at Siemens)
Sajal Ghosh *synaptic vesicles* (now at UCSD)

Andre Beerlink *bilayer imaging* (now at DESY)

Sebastian Kalbfleisch *P10-GINIX* (now at NSLSII, Brookhaven Natl. Lab.)
Christian Oldendrowitz *imaging of multicellular organisms / neuroscience* (now at Bruker)

Marius Priebe *cellular imaging and diffraction, cryo imaging*
Markus Osterhoff *numerical optics, focusing, mirror design*
Henrike Neubauer *waveguide optics and fabrication*
Sven Krüger *waveguide optics and fabrication* (now at ZF)

Britta Weinhausen, Sarah Köster, Institut für Röntgenphysik

Michael Sprung, HASYLAB
Ana Diaz, Pierre Thibault, Franz Peiffer cSAXS /SLS , TUM
Peter Cloetens, Heikli Suhonen, Id22ni
Manfred Burghammer, Id13

funding:
SFB 755 Nanoscale Photonic Imaging
SFB 937 Collective Behavior of Soft and Biological Matter
SFB 803 Functionality by organisation of membranes…
EXC-172 Molecular physiology of the brain

SFB 755 SFB 937 SFB 803 DESY

Classical radiology

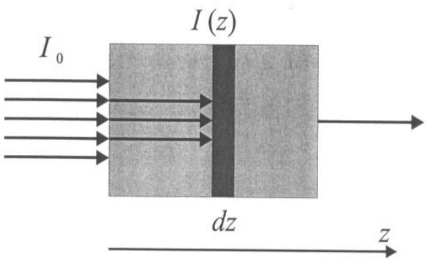

$$I(z) = I_0 e^{-\mu z}$$

absorption coefficient

$\mu \sim E^{-3} \quad Z^{+4}$

~1896

Study bulk structures using simple projections or tomography

object | projection | sinogram | 2D slice | 3D-Object

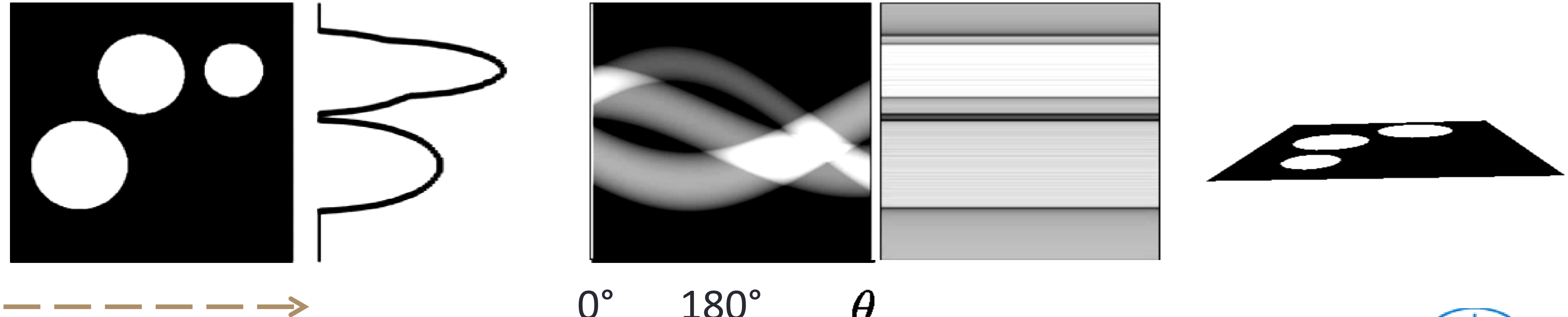

0° 180° θ

x-ray beam

animations by M. Bartels

X-ray shadow microscopy

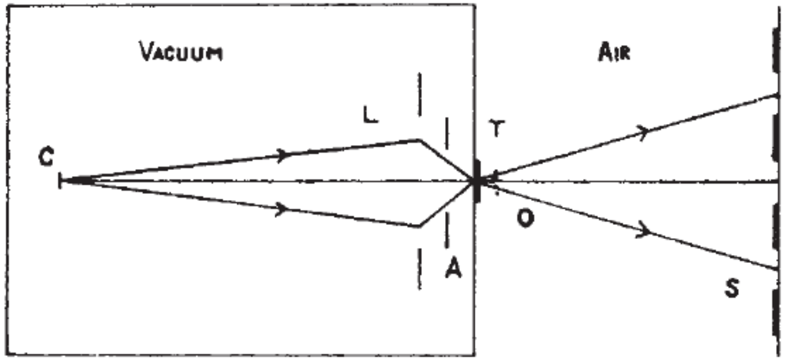

Fig. 1. Principle of X-ray shadow microscope

NATURE July 7, 1951 VOL. 168

e or less
ere is no
rial near
trip.
tially on
ve oxide,
potential
ietal and
resents a
ate equi-
of very
ubstrate.
orted in
nd liquid
xide and
equilibria
solid iron
he oxide
e higher
roduct is
that the

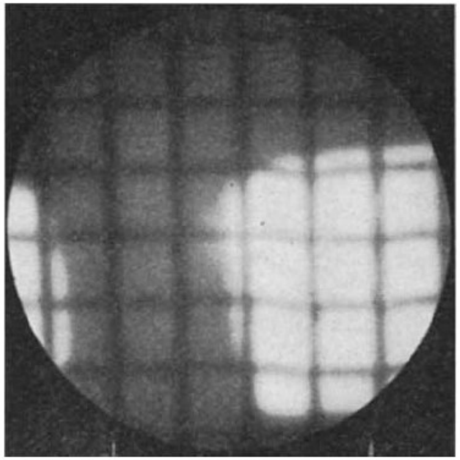

← 100 μ →

Fig. 2. X-ray shadowgraph of silver grid (1,000 mesh/in.) overlapping copper grid (200 mesh/in.). Original magnification, ×95; final magnification, ×285

No. 4262 July 7, 1951 NAT

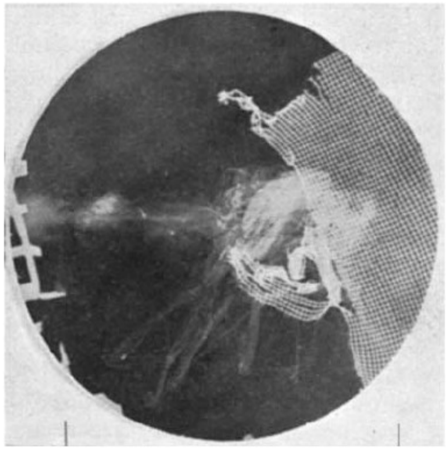

← 1 mm. →

Fig. 3. X-ray shadowgraph of book louse (*Liposcelis granicola*) and silver grid of 1,500 mesh/in. Original magnification, ×25; final magnification, ×37

The shadow of the object is magnified on the Detector / film by simply using a divergent beam. The resolution is limited by the source size to about 1µm.

Shadow microscopy with 3rd generation sources

- Smaller effective source size / focusing optics
  - ➢ Higher resolution is possible
  - ➢ Resolution beyond detector pixel size is achieved

- Higher intensity and tunable wavelength
  - ➢ Better statistics, weakly scattering samples, dynamics?
  - ➢ Contrast can be tuned / radiation damage minimized

- Coherence
  - ➢ Wave field contains additional information that can be exploited
  - ➢ Different techniques become possible, e.g. holography

- Digital data treatment
  - ➢ Allows for „reconstruction“ of the object from the measured intensity pattern which is not necessarily a real space image of the sample

Goals and methods

Structural biophysics

- **biomolecular assembly**
- **from in-vitro to cells and organismns**
- **3D spatial arrangement**

X-ray

- **field-of view / 3D**
- **Quantitative contrast**
- **resolution**

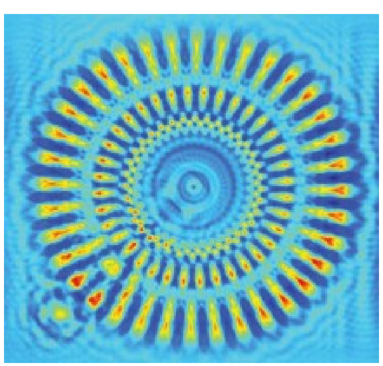

(nano)-diffraction

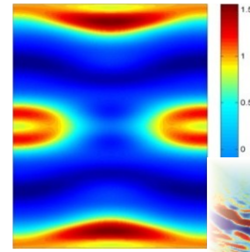

biomolecular assemblies

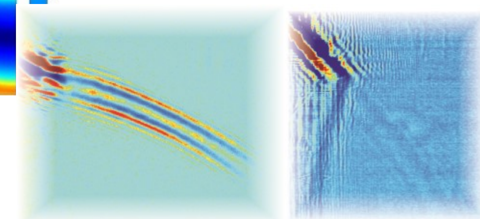

ptychography

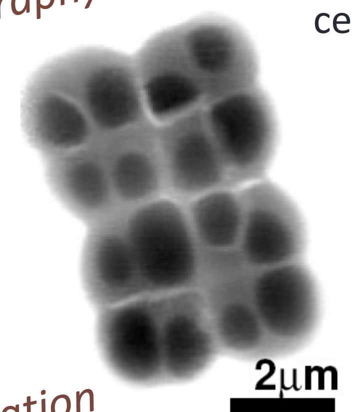

cells

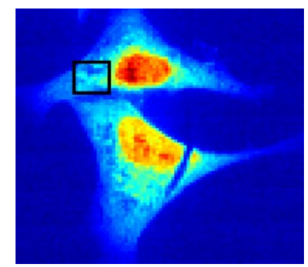

propagation imaging

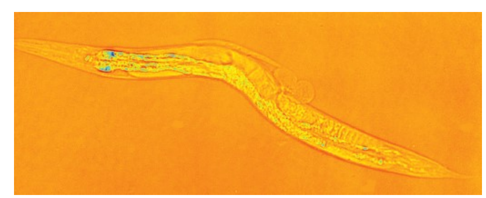

tissue / organs

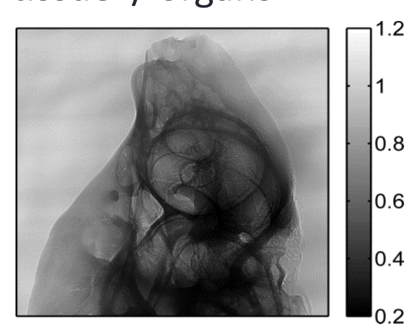

µ-focus CT (lab)
Talbot

Res	FoV
0.5nm	50nm
50nm	5µm
0.5µm	500µm
5µm	5mm

Priciple of propagation imaging

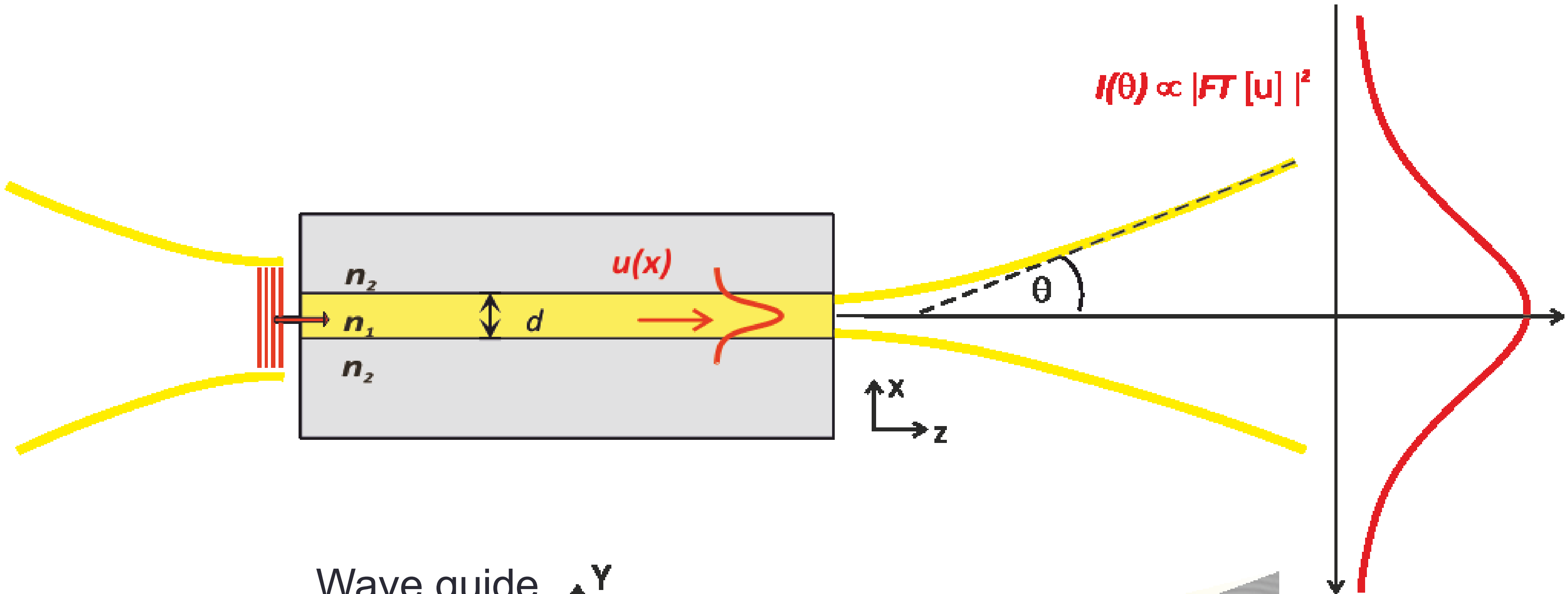

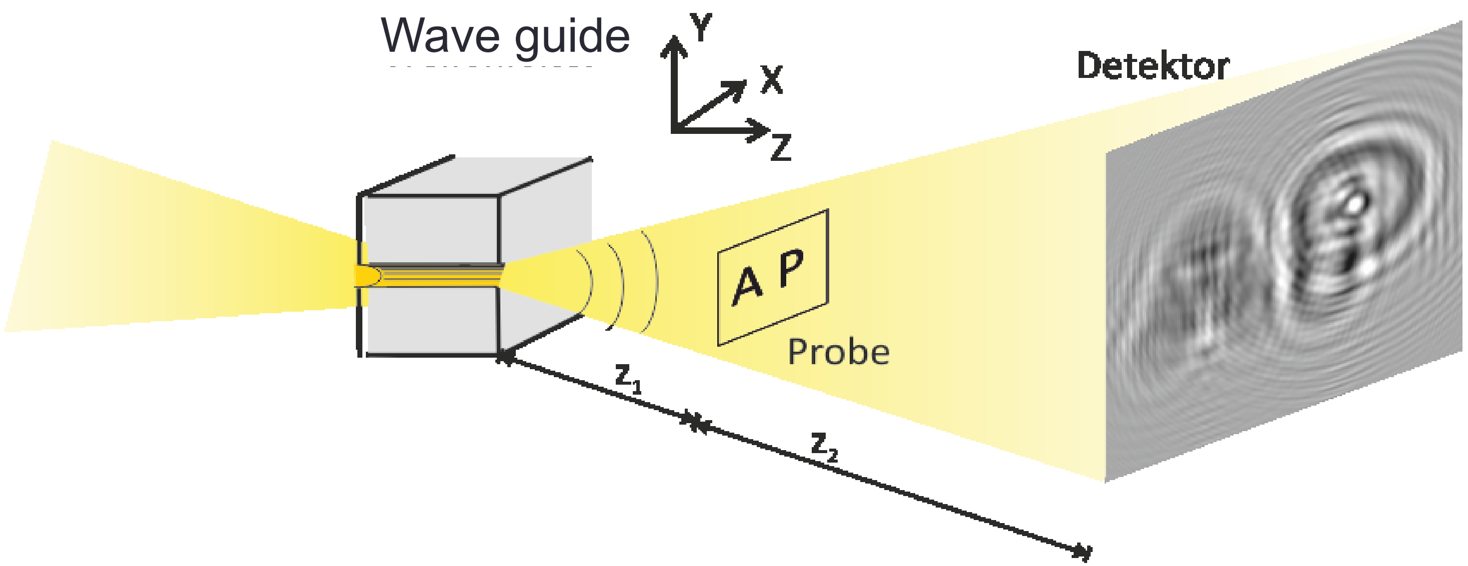

Priciple of propagation imaging

Fresnel scaling theorem:

an equivalence between parallel and point source illumination

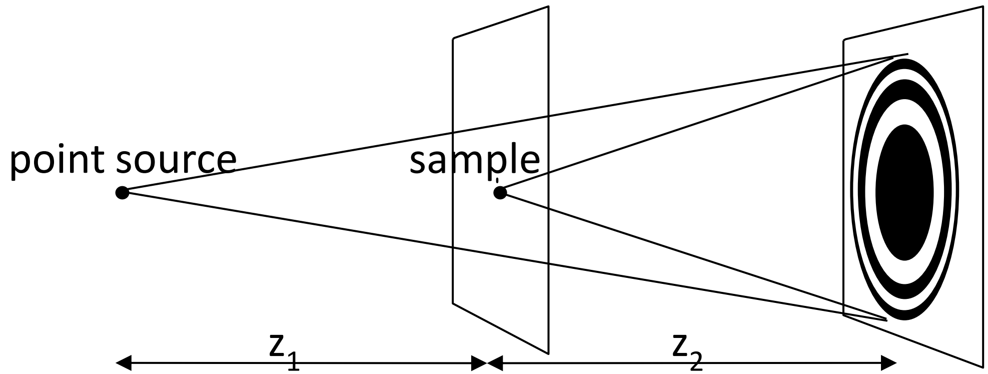

hologram recorded with the point source corresponds to a hologram recorded with a plane wave at an effective defocusing distance

$$z_{eff} = \frac{z_1 z_2}{z_1 + z_2}$$

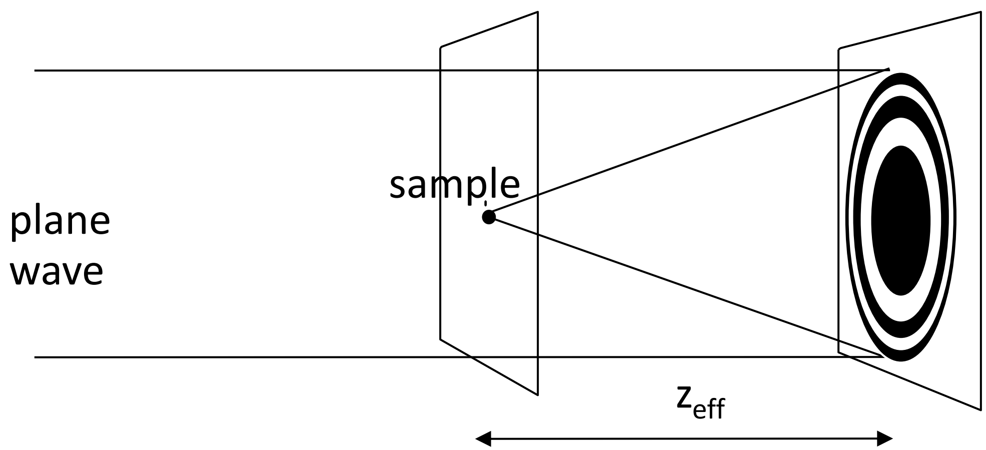

magnified by

$$M = \frac{z_1 + z_2}{z_1}$$

→magnification allows for a spatial resolution below detector pixel size!

→ plane wave setup used for simulations and reconstruction

Schematics of the setup

Göttingen **I**nstrument for **N**ano **I**maging with **X**-rays
@ P10, PETRA III, Hamburg

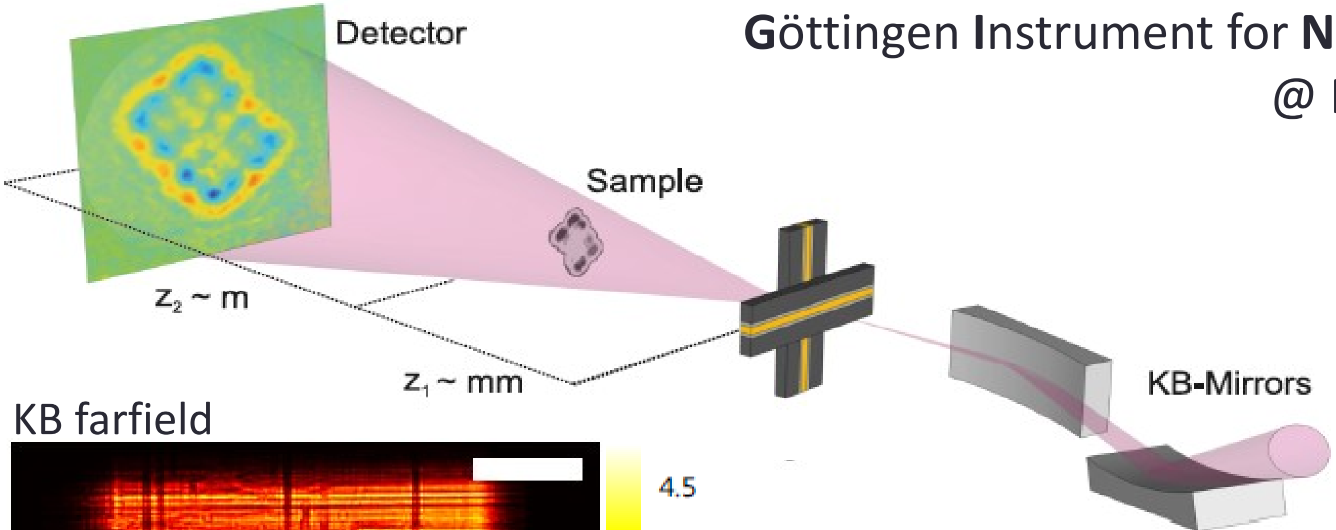

200 nm x 200 nm
$>10^{11}$ ph/s

KB farfield

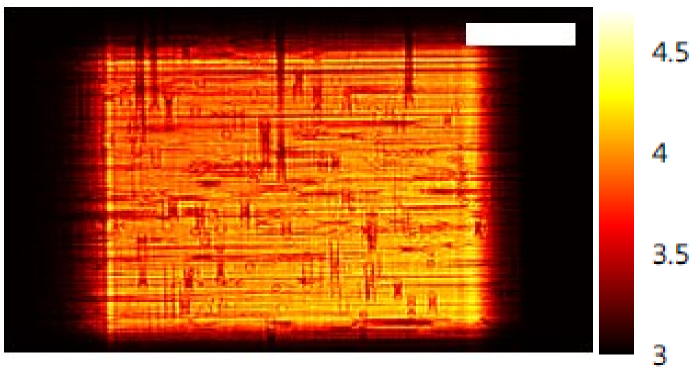

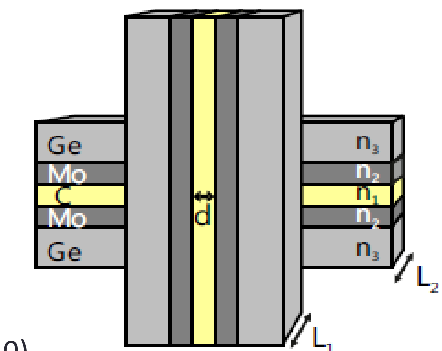

10 nm x 10 nm
10^7 -10^8 ph/s
13-15 keV

Krüger et al. Opt. Express **18**, 13492 (2010)
Krüger et al. J. Synchrotron. Rad. **19**, 227 (2012)

Waveguide farfield

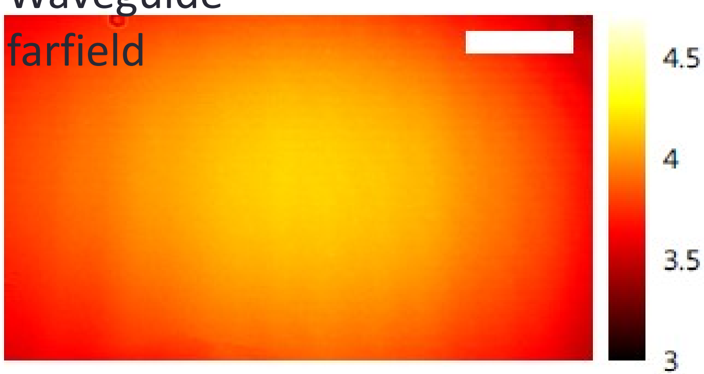

20 nm x 17 nm
$2x10^9$ ph/s
8 keV

H. Neubauer, Doktorarbeit 2012
J. Haber, Masterarbeit 2013

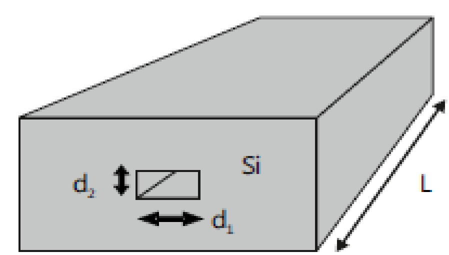

GINIX setup @ P10

Propagation of the wave field and image formation

$$\psi(x',y',z)=\frac{1}{i\lambda}\int_{-\infty}^{\infty}\int_{-\infty}^{\infty}\psi(x,y,0)\frac{1}{r}\exp(ikr)\frac{1+\cos(\vec{n}\cdot\vec{r})}{2}dxdy \qquad \psi(x,y,0)=\psi_0\,\tau(x,y)$$

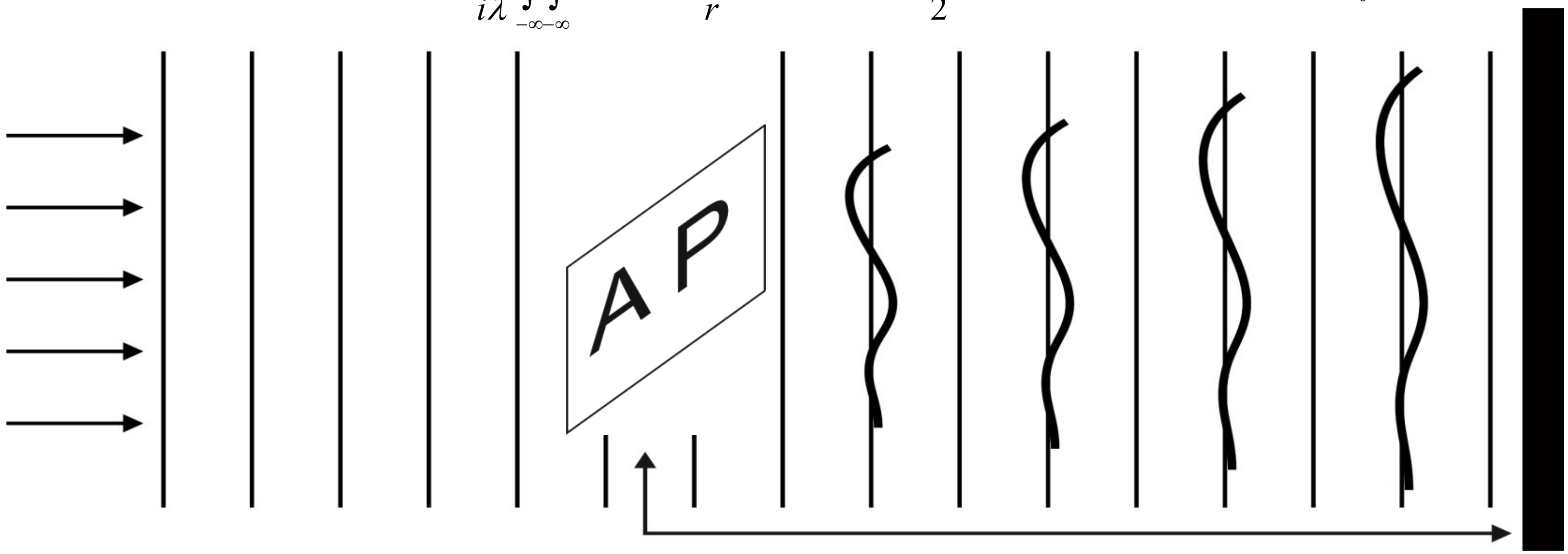

$$\psi_z = FT^{-1}[\exp[iz\sqrt{k^2-k_x^2-k_y^2}]\,FT[\psi_0]]$$

object with complex transmission function $\tau(x,y)$

Absorption Phase

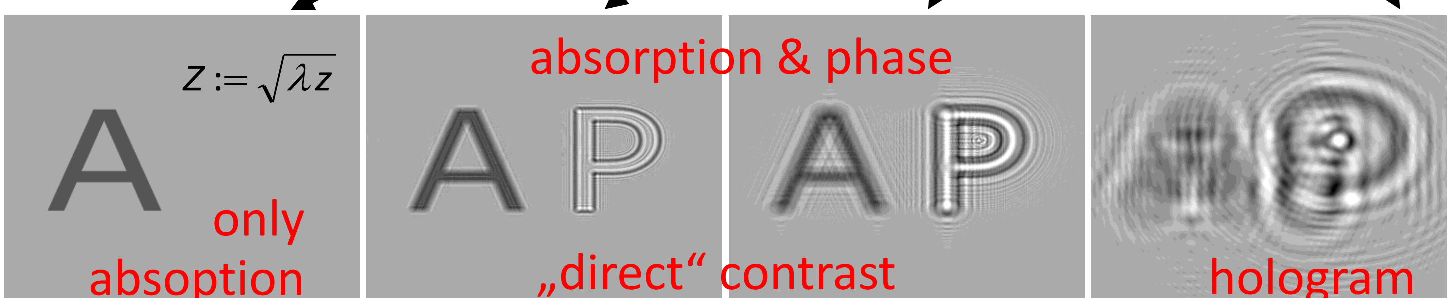

Propagation imaging pioneered by: P. Cloetens et al. et al. 1999; S.Wilkins et al., 2000-2004

Gabor-type holography – In-line holography

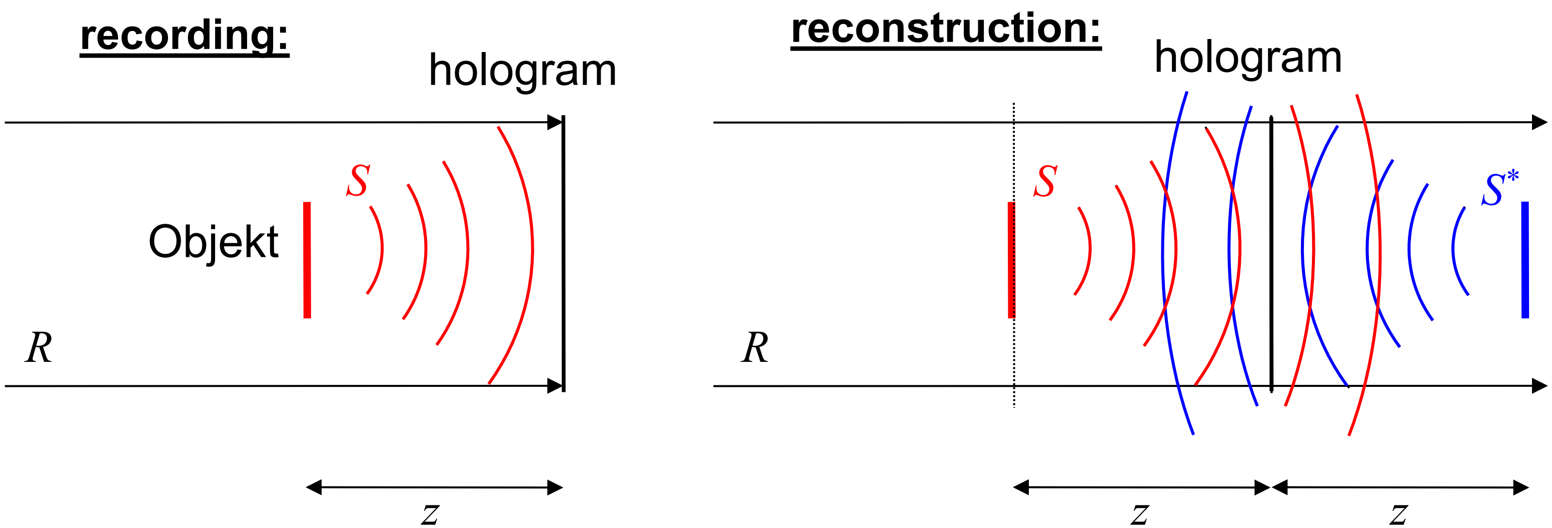

reference beam

signal

conjugated wave
„twin image“

$$\phi(x,y) = 1 + \tau(x,y)$$

$$\tau \xrightarrow{D_z} \tilde{\tau} = D_z[\tau]$$

$$I(x,y) \propto |1+\tilde{\tau}|^2 = 1 + \tilde{\tau} + \tilde{\tau}^* + |\tilde{\tau}|^2$$

$$\tau_{recon} = D_{-z}[1 + \tilde{\tau} + \tilde{\tau}^* + |\tilde{\tau}|^2] = 1 + \tau + \tau^* + D_{-z}\left[|\tilde{\tau}|^2\right]$$

issues:

- **reconstruction algorithms and twin image**
- **magnification and wavefront abberation**
- **normalisation of the measured intensity by empty beam**

Solving the phase problem – simulation

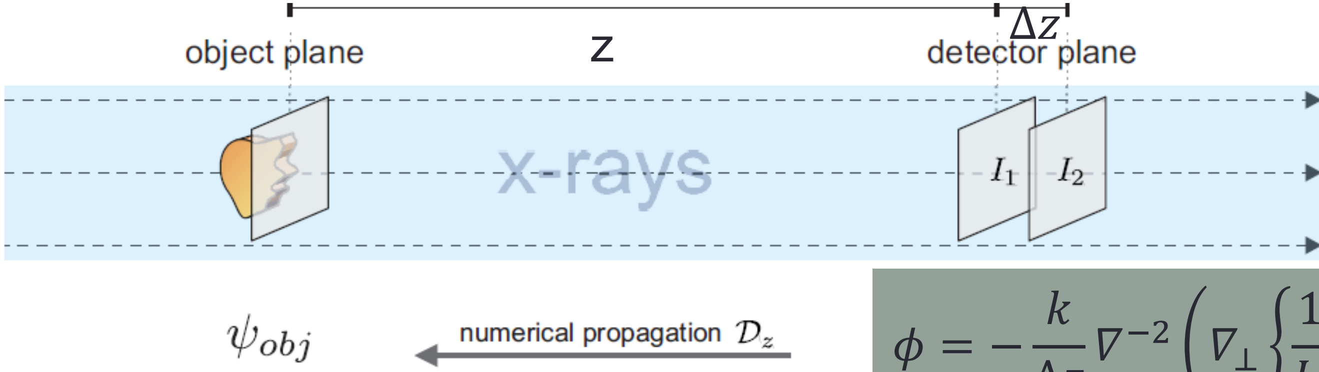

$$\phi = -\frac{k}{\Delta z} \nabla^{-2} \left(\nabla_\perp \left\{ \frac{1}{I_1} \nabla_\perp (\nabla_\perp^{-2} [I_1 - I_2]) \right\} \right)$$

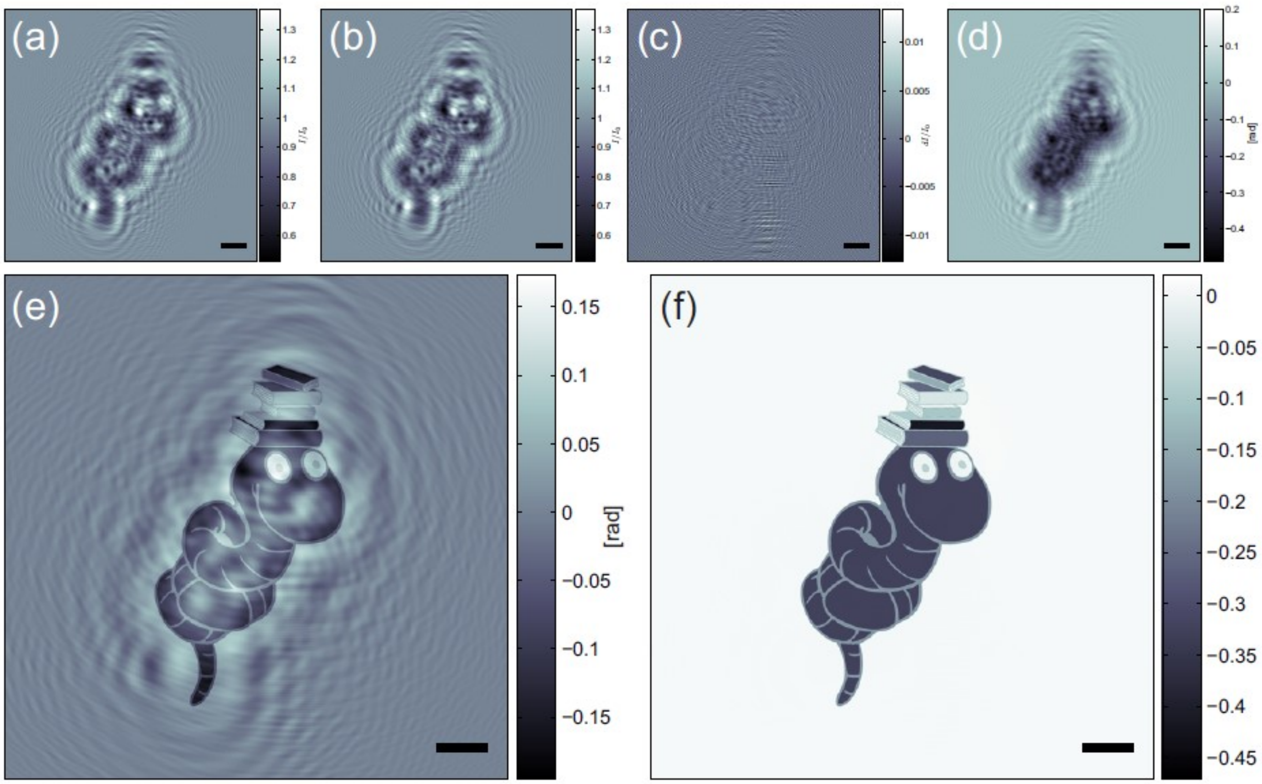

Approximate phase can be calculated and then be used for a better reconstruction

Opt. Expr. 21, 2220 (2013)

Solving the phase problem - experiment

sub-pixel drift correction

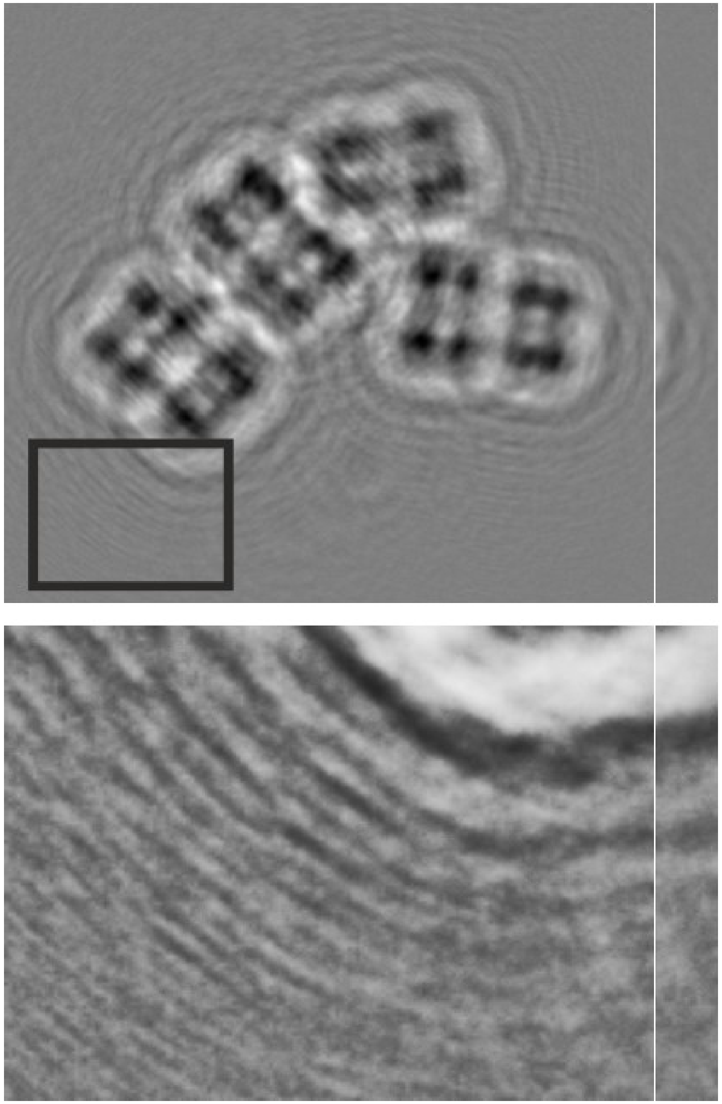

3distances

D. Radiodurans

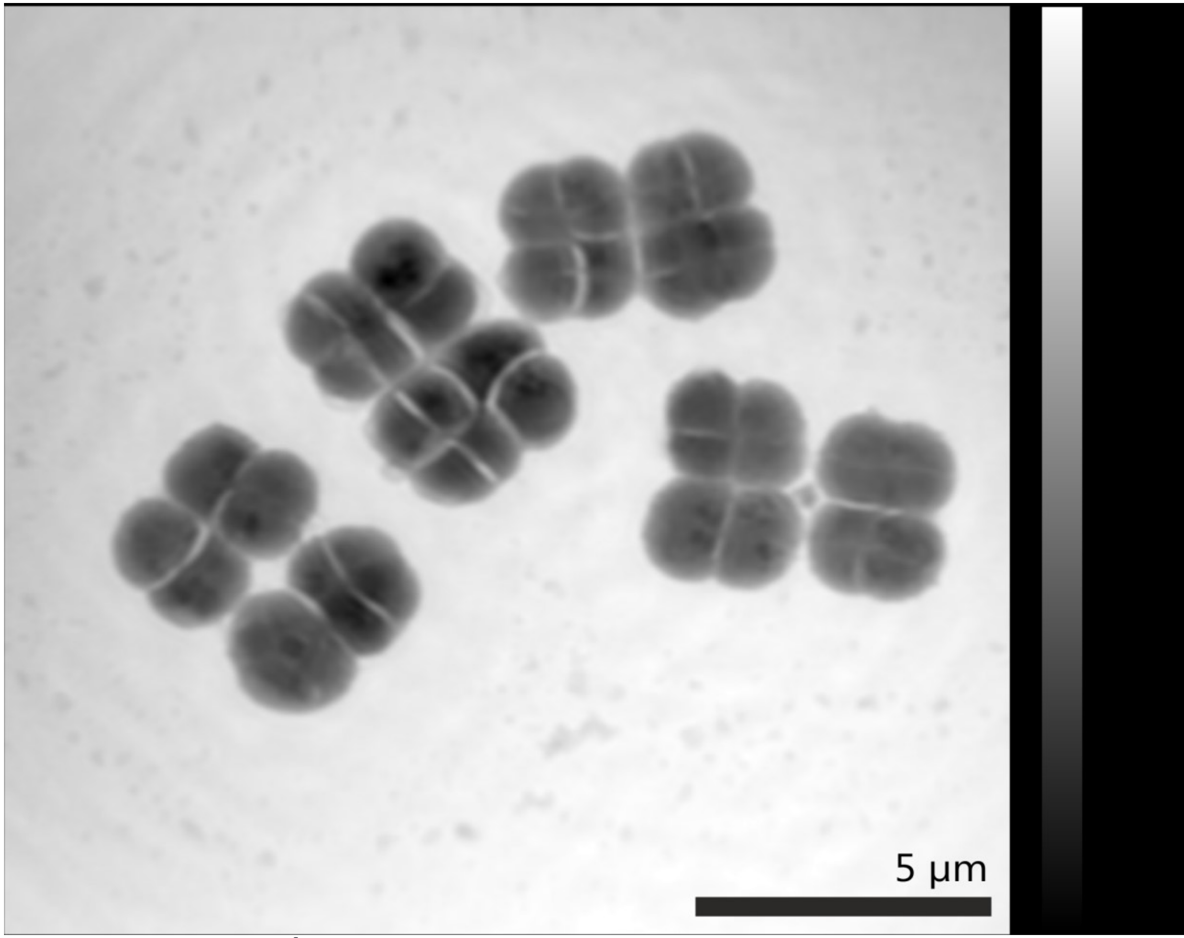

25 nm resolution
(17.5 µm)^2 FOV
1.3x10^5 Gy

Summary

- From radiography to coherent projection imaging
- High resolution imaging endstation at the coherence beamline P10
- Imaging of weakly scattering objects / biological cells via phase contrast imaging in the holographic regime
- A method to measure the phase via “Transport of Intensity Equation”

- Part II

Magnetic Holography

People and collaborations

DESY

L. Müller
M.H. Berntsen
S. Schleitzer
C. Gutt
M. Walther
G. Grübel
R. Treusch
A. Al-Shemmary
H. Redlin
S. Düsterer

Universität Hamburg

J. Bach
A. Kobs
K. Bagschik
B. Beyersdorff
R. Frömter
H.P. Oepen

UPMC Sorbonne Universités

B. Vodungbo
R. Delaunay
K. Li
J. Lüning

TU Berlin

B. Pfau
C.M. Günther
S. Schaffert
F. Büttner
F. von Korff Schmising
J. Geilhufe
S. Eisebitt

LCLS

A. Scherz
C. Graves
B. Wu
W. Schlotter
H. Dürr

Elettra Sincrotrone Trieste

F. Capotondi
E. Pedersoli
M. Kiskinova

LEXI
LANDESEXZELLENZINITIATIVE HAMBURG

SFB
SFB 925: Light induced dynamics and control of strongly correlated quantum systems

Imaging of magnetic domain patterns with X-rays

> X-ray lenses based methods

Scanning Transmission X-ray Microscopy
STXM

Transmission Imaging X-ray Microscopy
TIXM

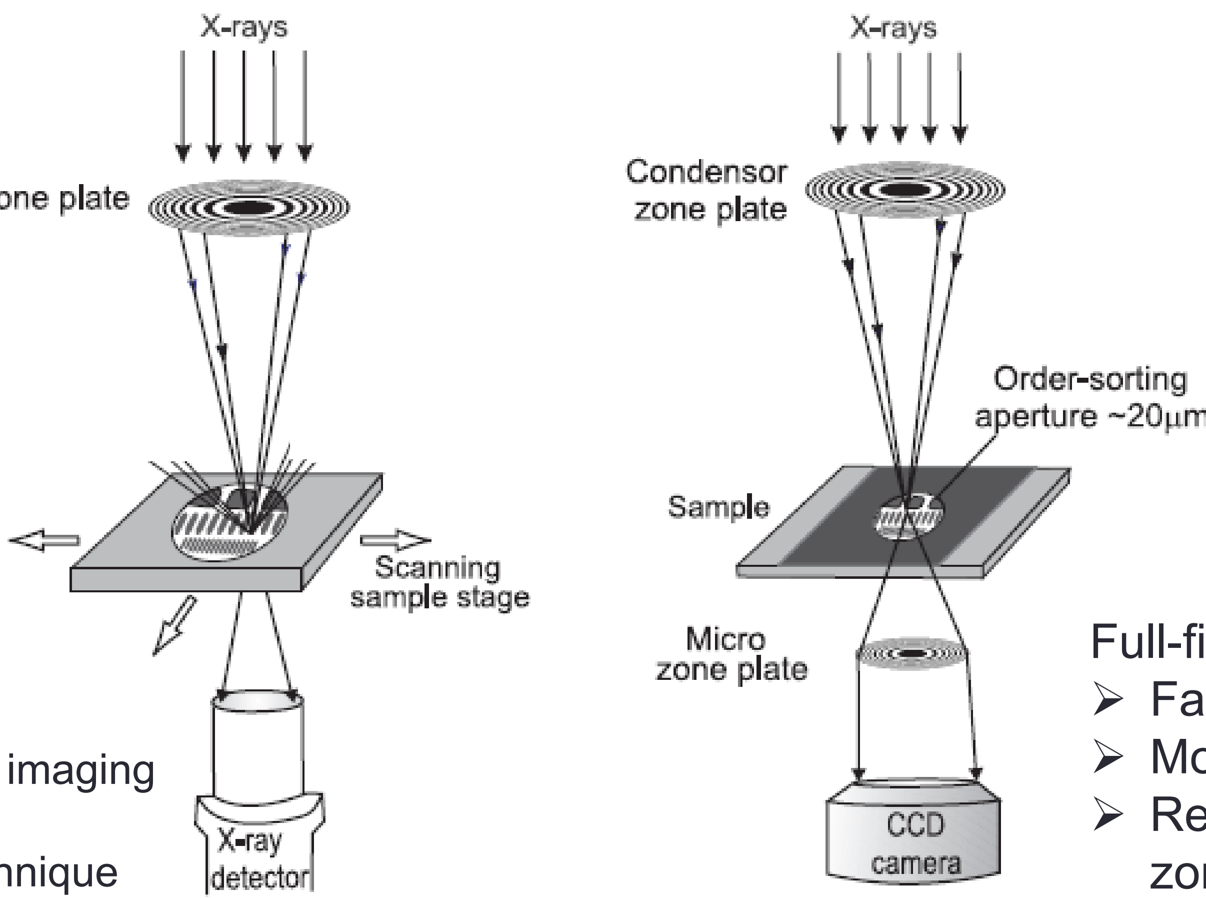

Point-by-point imaging
- Slow
- Simple technique
- Resolution limit = focal-spot size

Full-field microscopy
- Fast (detector limited)
- More difficult
- Resolution limit by zone plate

Imaging of magnetic domain patterns with X-rays

> X-ray lense-based method

See, e.g., X-Ray Data Booklet, Sec 4.4
http://www.x-ray-optics.de

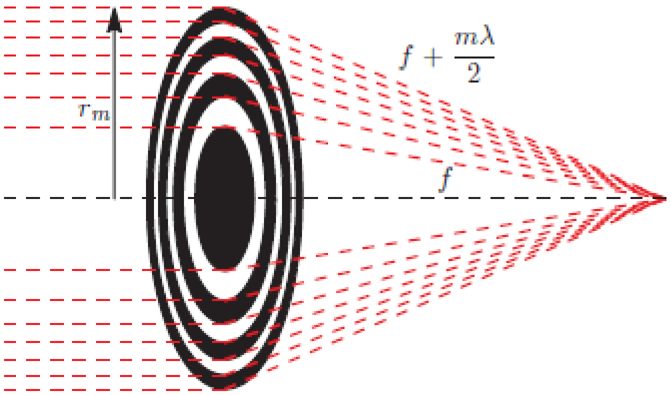

Fresnel Zone plates:
Condition for constructive interference at focal distance *f*

$$r_n = \sqrt{m\lambda f + \frac{m^2\lambda^2}{4}} \approx \sqrt{m\lambda f}$$

All zones have the same area

$$A_m = \pi(r_{m+1}^2 - r_m^2) = \pi\lambda f$$

Resolution determinded by width of outermost zone
$\Delta x = 1.22\Delta r_m \approx 10\text{nm}$ nowadays
(7.8 nm FWHM shown in 2017 [Sci. Rep. 7, 43624]).

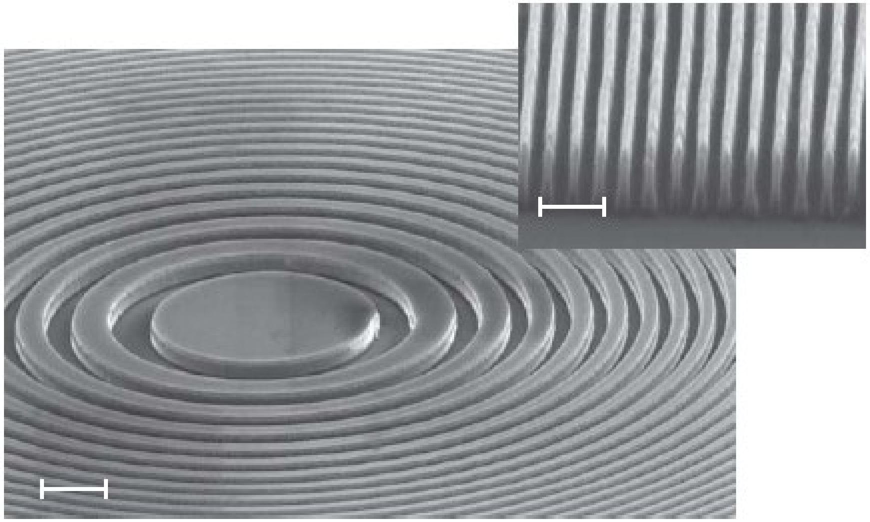

disadvantages:
- High absorption (5-30% efficiency)
- Hard to fabricate

Imaging of magnetic domain patterns with X-rays

> X-ray lense-based method

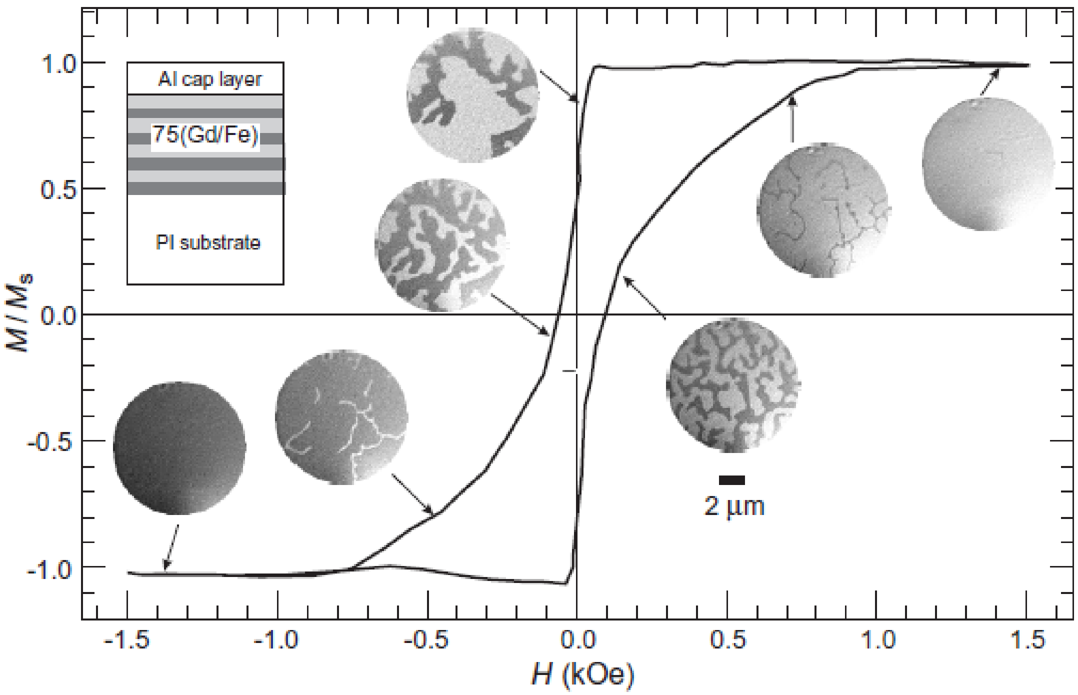

Fig. 10.22. TIXM images recorded at the FeL3-edge as a function of applied field for a 75 × [Fe(4.1 Å)/Gd(4.5 Å)] multilayer deposited on polyimide and capped for protection with an Al layer [463, 482]

- Element-sensitivity
- Integration of gray values for each field value
  ➔ hysteresis

Stöhr and Siegmann, Magnetism

Image the nanoscale – Fourier-transform holography

Usually, in a scattering experiment the phase is lost – only the intensity is recorded

However, in a simple scattering pattern we know the phase

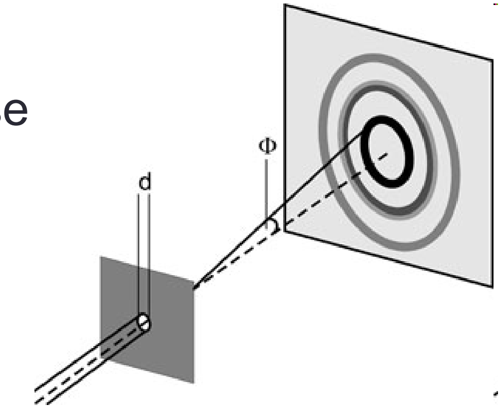

Now, lets use that to encode the scattering pattern of a more complicated (strongly scattering) object

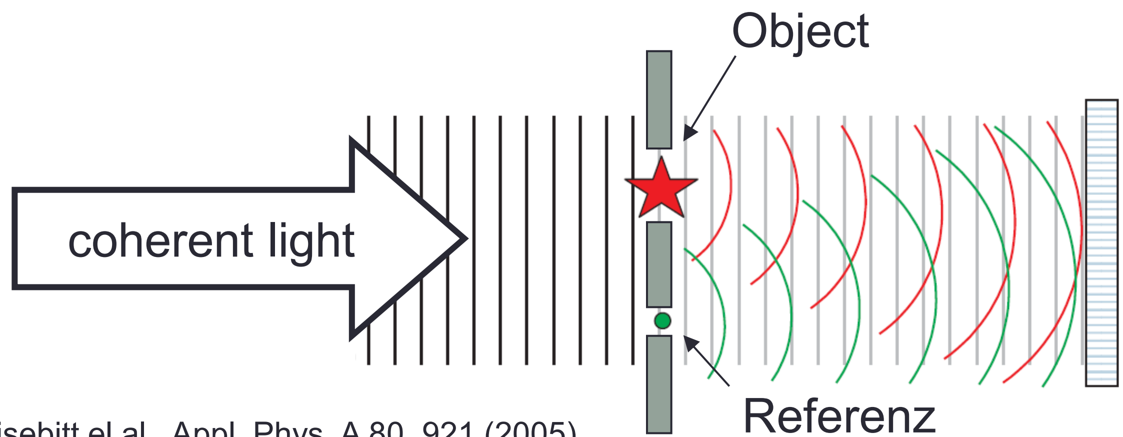

detector

$$I = |A(\mathrm{obj}) + A(\mathrm{ref})|^2$$

S. Eisebitt el al., Appl. Phys. A 80, 921 (2005)

Object and reference wave interfere on the detector if object and reference are illuminated coherently and the (polarization) state of the light is not changed by the scattering…

Image the magnetic nanoscale – magnetic FTH

… unfortunately, magnetic scattering does exactly that with linear light

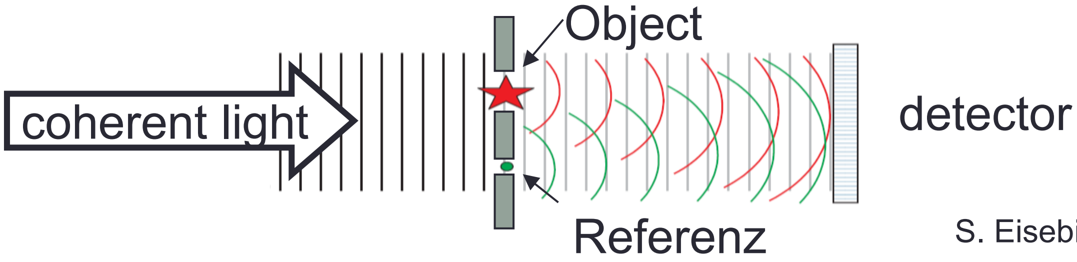

$$I_{\text{lin}} = |A(\text{obj})|^2 + |A(\text{ref})|^2$$

S. Eisebitt el al., Appl. Phys. A 80, 921 (2005)

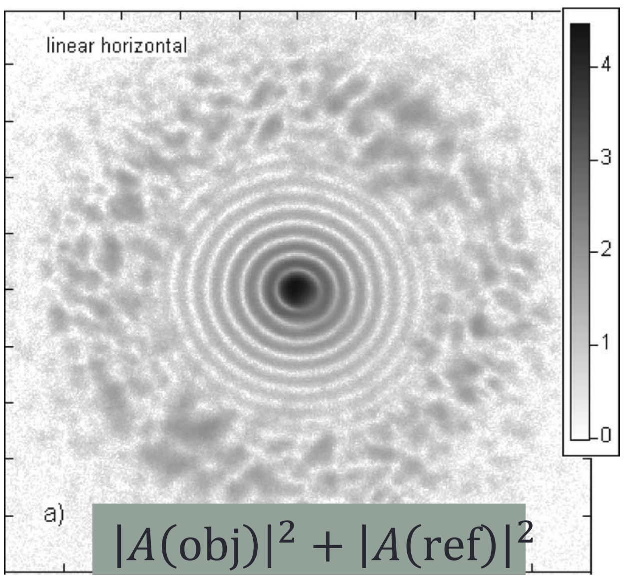

Linear light

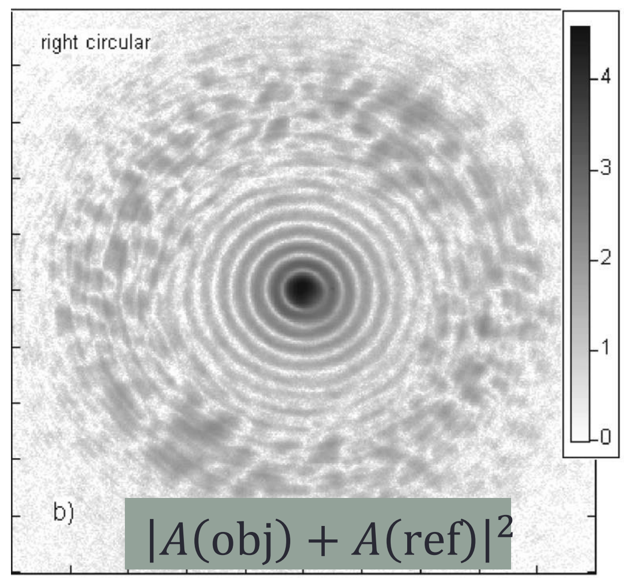

Circular light

S. Eisebitt et al., PRB, **68** 104419 (2003).

FTH image formation

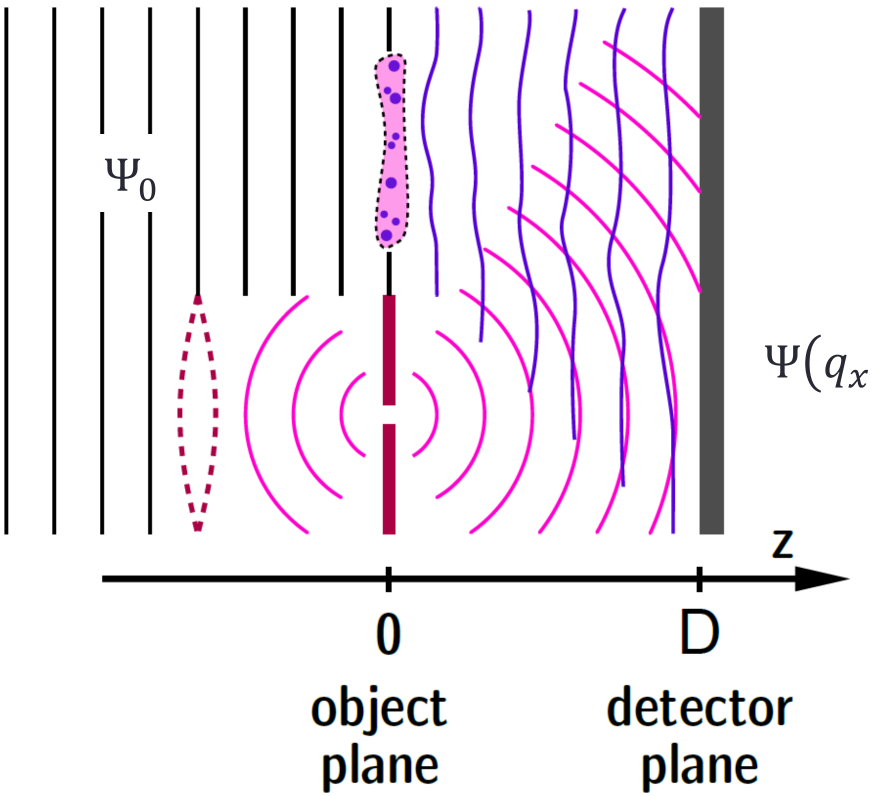

- Sample transmits incoming wavefield $\Psi(x,y) = t(x,y)\Psi_0$
- In the far field $\left(F \ll 1, F = \frac{\ell^2}{D\lambda}\right)$ one masures a Frauhofer pattern described by

$$\Psi(q_x, q_y) = \iint_{-\infty}^{\infty} \Psi(x,y) \exp\left(-i\left(q_x x + q_y y\right)\right) \, \mathrm{d}x\mathrm{d}y$$

This is the Fouriertransform of the transmitted wavefield which again is directly related to the sample structure.

- Unfortunately we measure the absolute square of the wavefield and the phase is lost. Hence we get

$$\begin{aligned} p(r') &= F^{-1}\{F^*(\Psi(r))F(\Psi(r))\} \\ &= \Psi^*(-r) * \Psi(r) \\ &= \iint_{-\infty}^{\infty} \Psi^*(-r)\Psi(r+r')\mathrm{d}r \end{aligned}$$

$p(r')$ is the spatial autocorrelation function or the Patterson map

What does the Patterson map tell us?

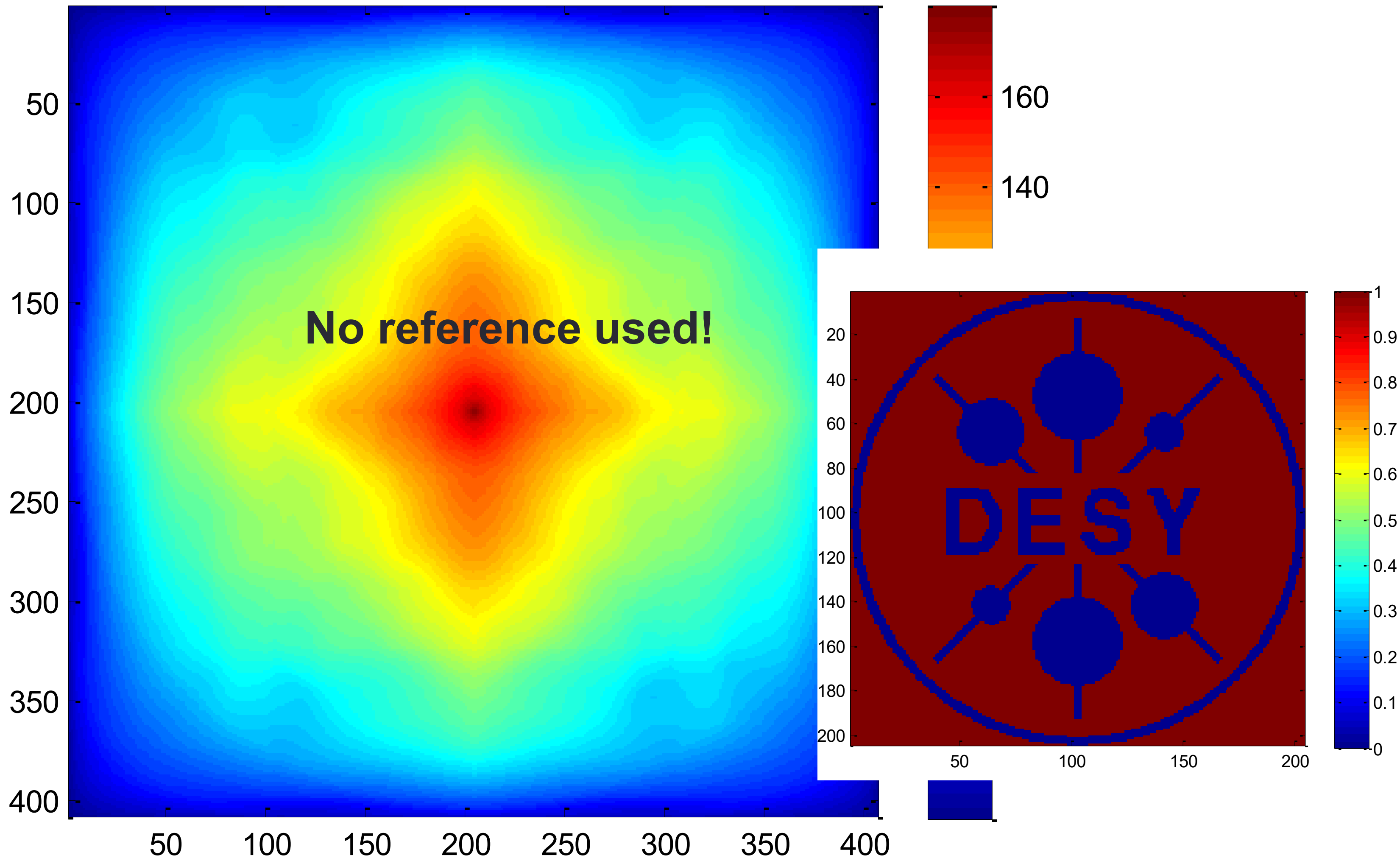

The trick of the reference

- No reference
- With reference

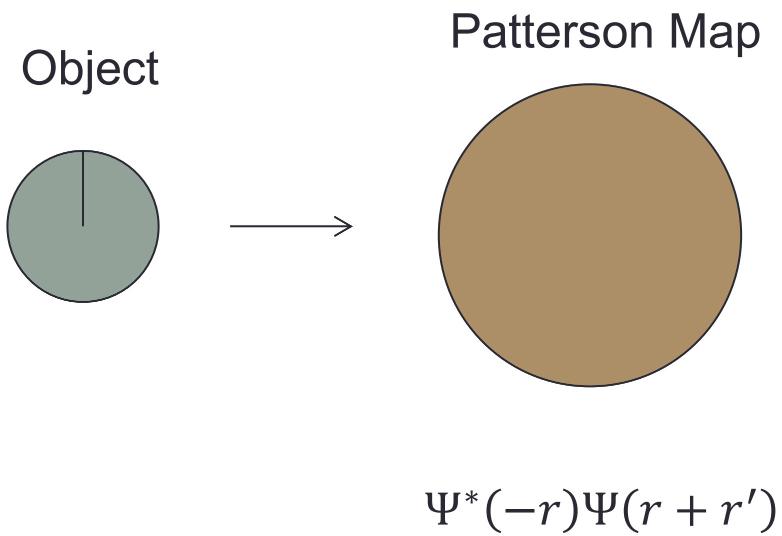

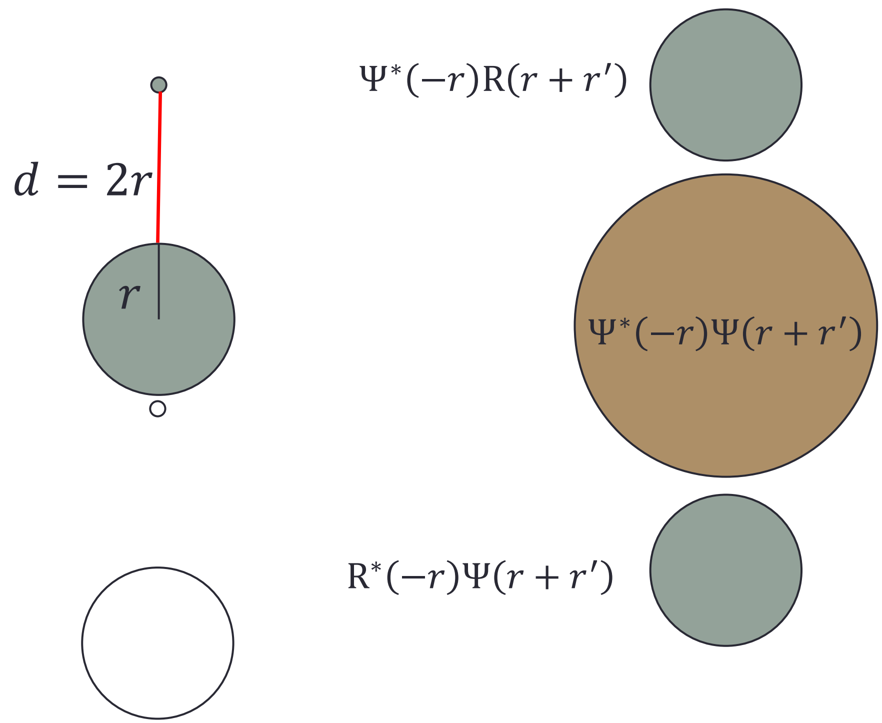

Needs iterative phase retrieval
Not necessarily easy

Real space image comes from FFT
Resolution limited by reference size

Imaging of magnetic domain patterns with X-rays

> Lensless Imaging – Fourier transform Holography

	Schlüsselelement-Herstellung		Bild-Rekonstruktion	
TXM	Zonenplatte	XXXXX	-direkt-	X
FTH	Optikmaske	XX	Einfache Fourier-Transformation	XX

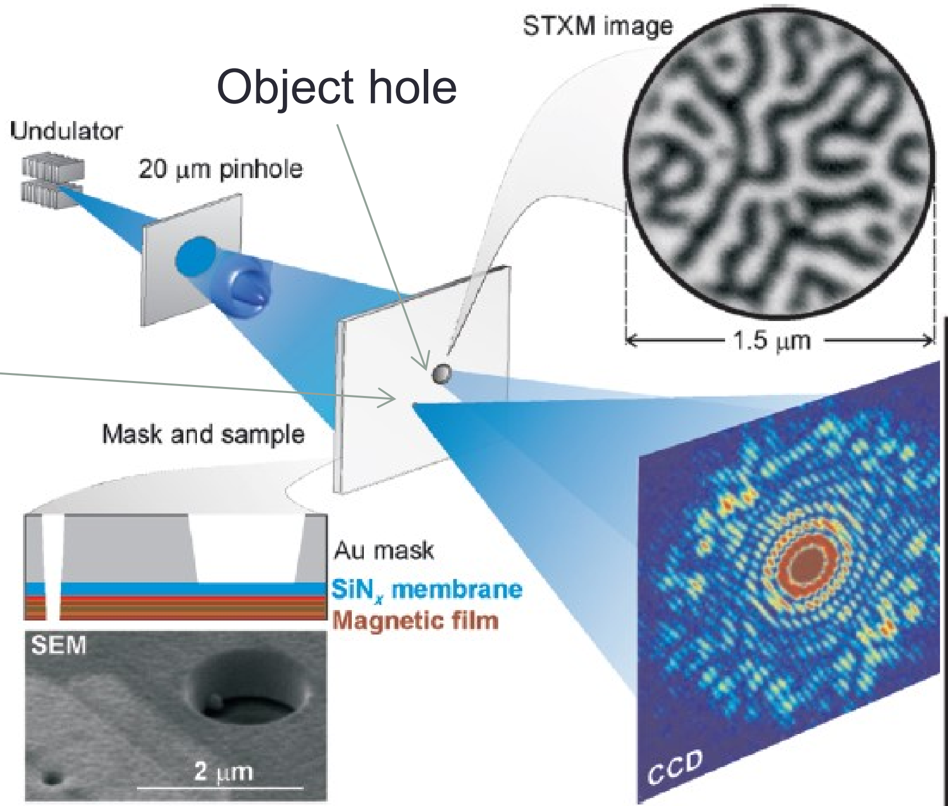

Requirement: transversal coherence length > largest length scale in sample = mask

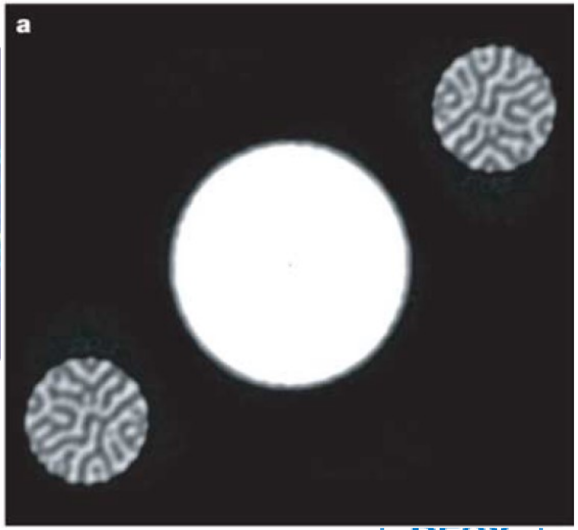

Imaging of magnetic domain patterns with X-rays

> Lensless Imaging – Fourier transform Holography

Mask and sample:

Preparation by focused ion beam technique

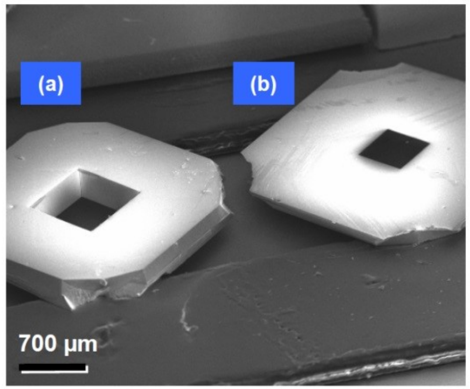

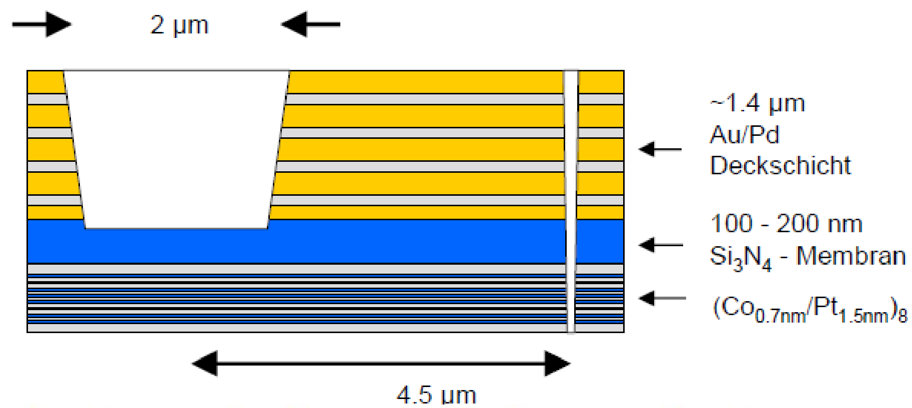

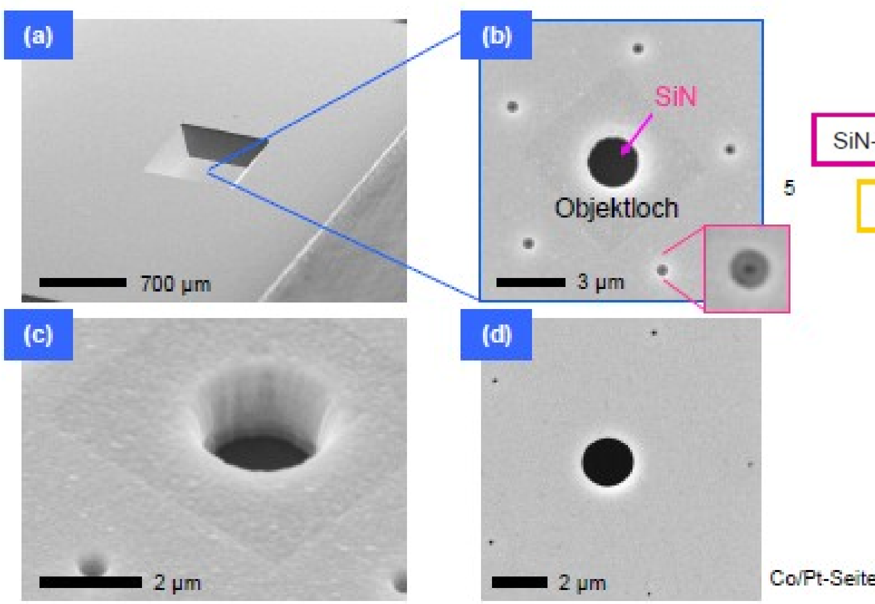

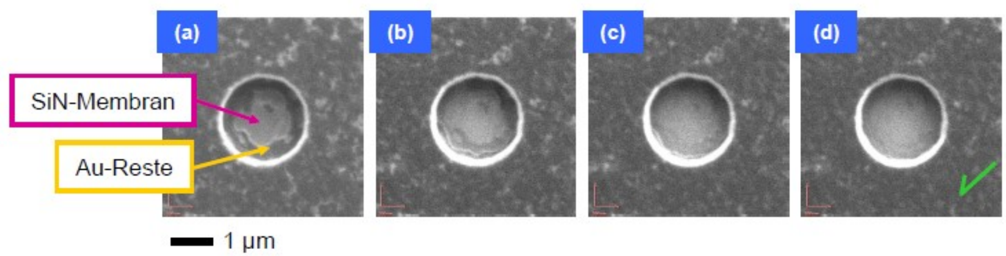

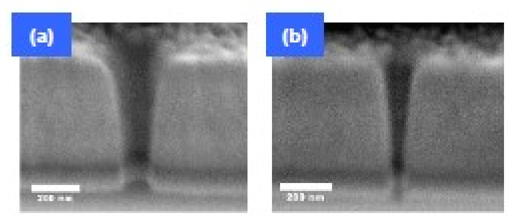

Imaging of magnetic domain patterns with X-rays

> Lensless Imaging – Fourier transform Holography (FTH)

Principle:

- Intensity on detector:

$$\mathrm{I}(q_x, q_y) = \left| \iint_{-\infty}^{\infty} \Psi(x,y) \exp\left(-i\left(q_x x + q_y y\right)\right)\, \mathrm{d}x\mathrm{d}y \right|^2$$

$\Psi(x,y) = t(x,y)\Psi_0, \Psi_0$ =illuminating wave (plane wave)

Transmission function

$$t(x,y) = \exp\left(\frac{2\pi}{\lambda}\int_0^d \left(-i\delta(x,y,z) - \beta(x,y,z)\,\mathrm{d}z\right)\right)$$

With δ and β from $\mathrm{n} = 1 - \delta + \beta$ and for magnetic samples $\delta = \delta_0 \pm (\epsilon_k \cdot \vec{m})\Delta\delta$ and $\beta = \beta_0 \pm (\epsilon_k \cdot \vec{m})\Delta\beta$

Identify t(x,y) as $f = f_0^C + f_r^C + f_m$

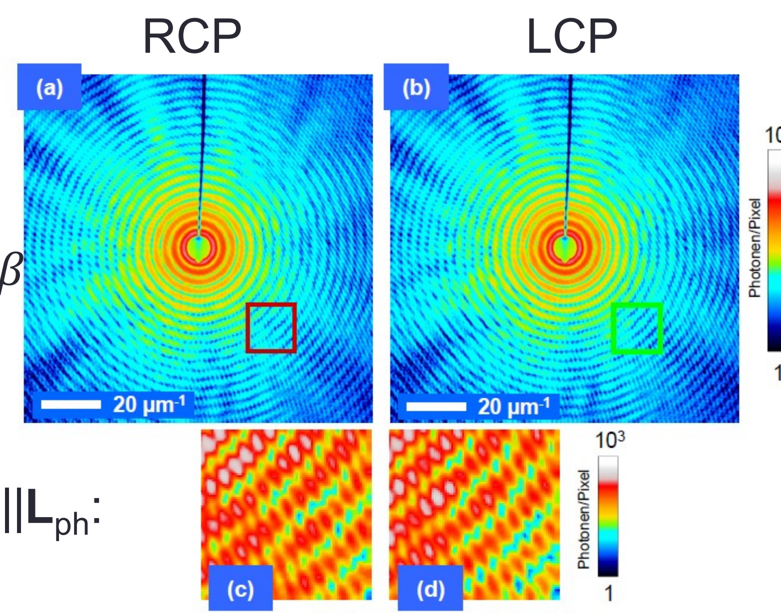

- Scattering factor for circularly polarized light and **M||L**$_{ph}$:

$$I(\vec{Q}) = \left|\tilde{f}_0^C(\vec{Q}) + \tilde{f}_r^C(\vec{Q}) \pm \tilde{f}_m(\vec{Q})\right|^2 = \left|\tilde{f}_C \pm \tilde{f}_m\right|^2$$

$$\Delta I = I(RCP) - I(LCP) = 2 \cdot \left(\tilde{f}_C^* \tilde{f}_m + \tilde{f}_C \tilde{f}_m^*\right)$$

Subtle differences!

Imaging of magnetic domain patterns with X-rays

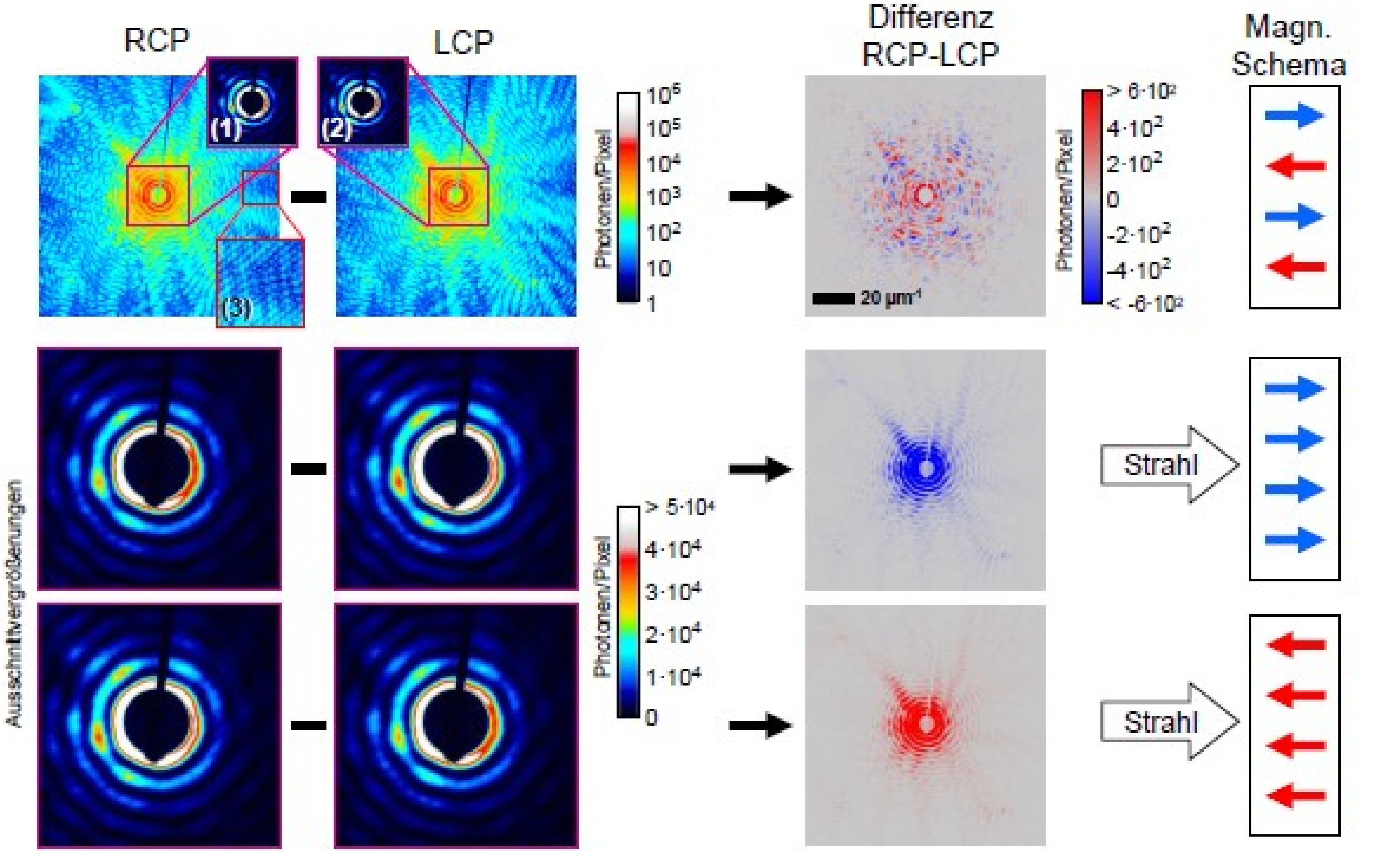

DESY

Imaging of magnetic domain patterns with X-rays

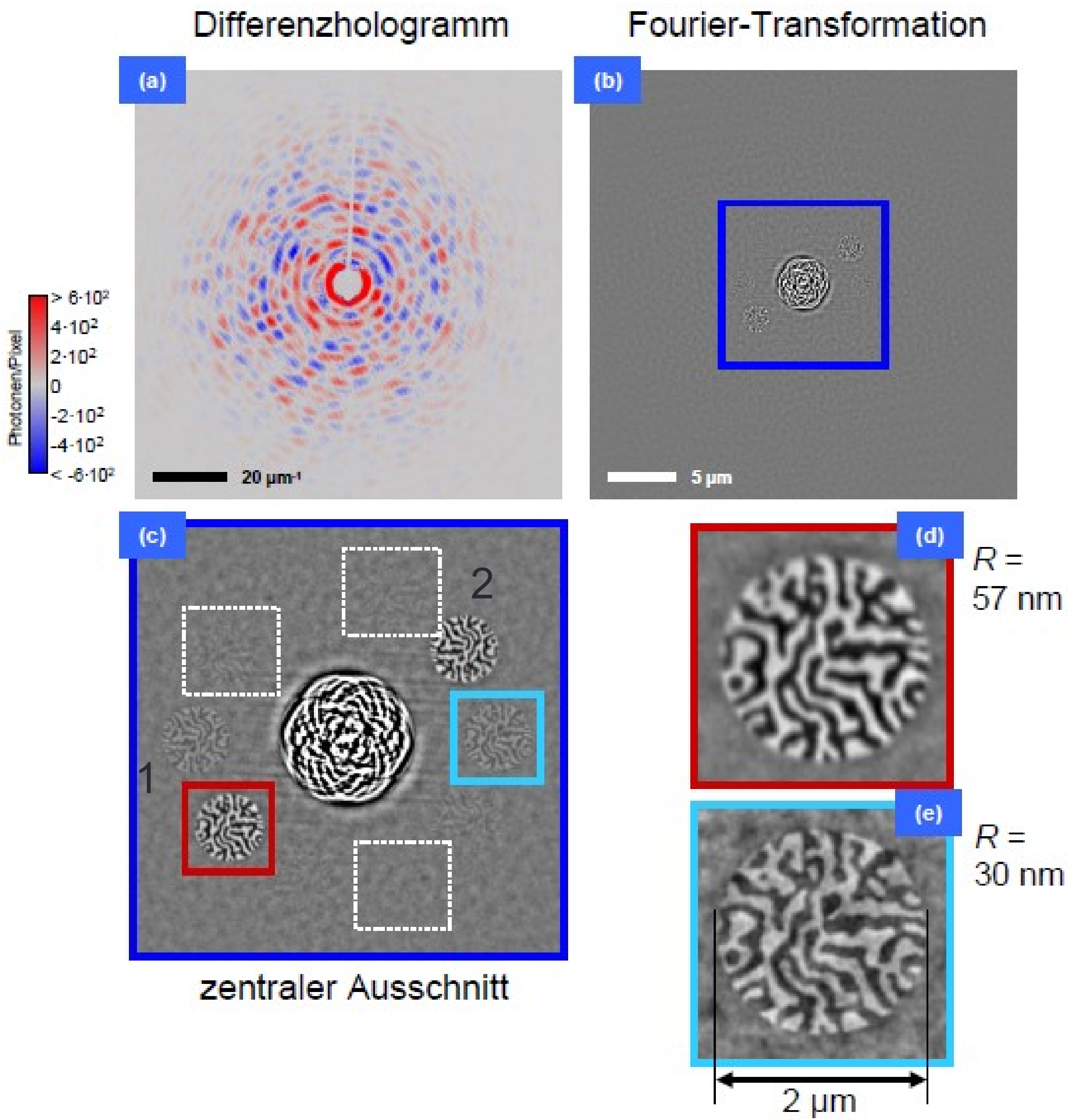

The FT of the Hologram shows the Patterson map of the Holographic mask with the magnetic structure. In the center there is the object-hole autocorrelation. The 10 reference-hole-object-hole cross correlations (2 for each reference hole) are aranged outside of that area. Large references yield high contrast but low resolution whereas small reference holes yield high resolution at low contrast.

Imaging of magnetic domain patterns with X-rays

> Lensless Imaging – Fourier transform Holography (FTH)

References holes with different inclinations

In-plane contrast:

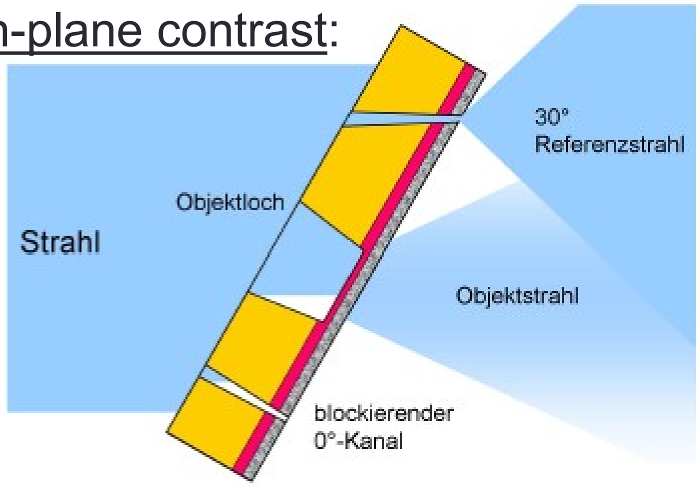

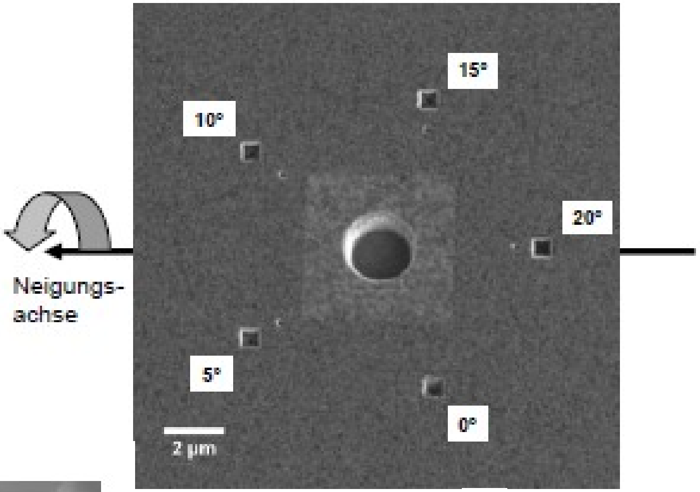

In-plane magnetized 20 nm thick Co film

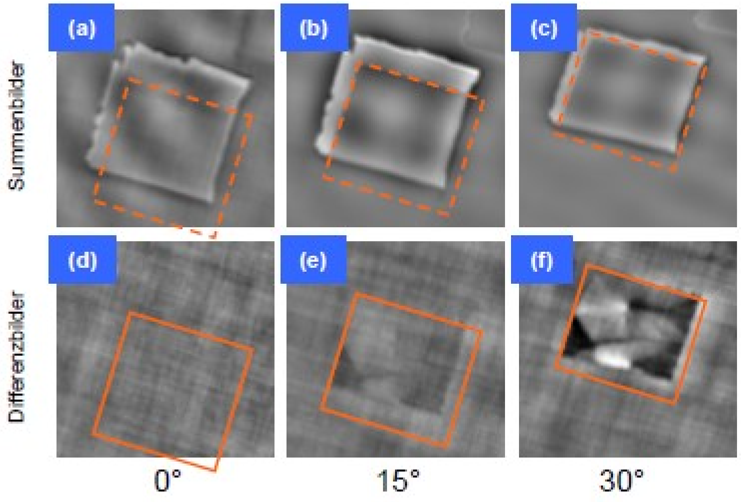

$$\Delta I_{XMCD} \propto \vec{M} \cdot \vec{L}_{\gamma}$$

> Lensless Imaging – Fourier transform Holography (FTH)

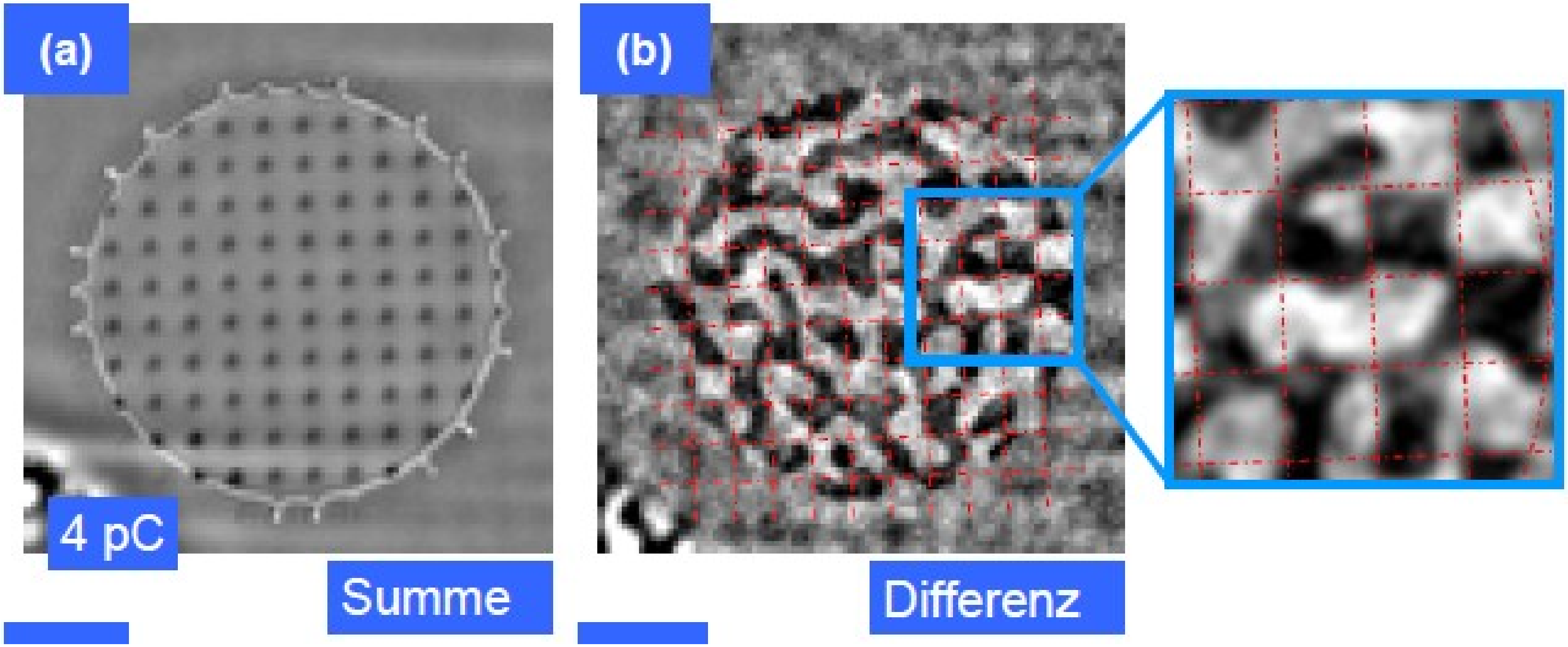

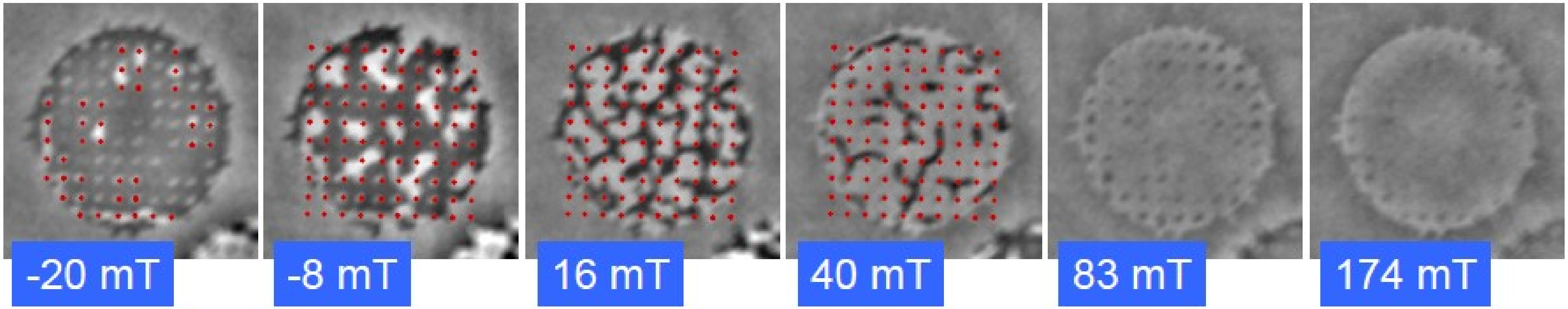

Imaging of magnetic domain patterns with X-rays

> <u>Lensless Imaging – Fourier transform Holography (FTH)</u>

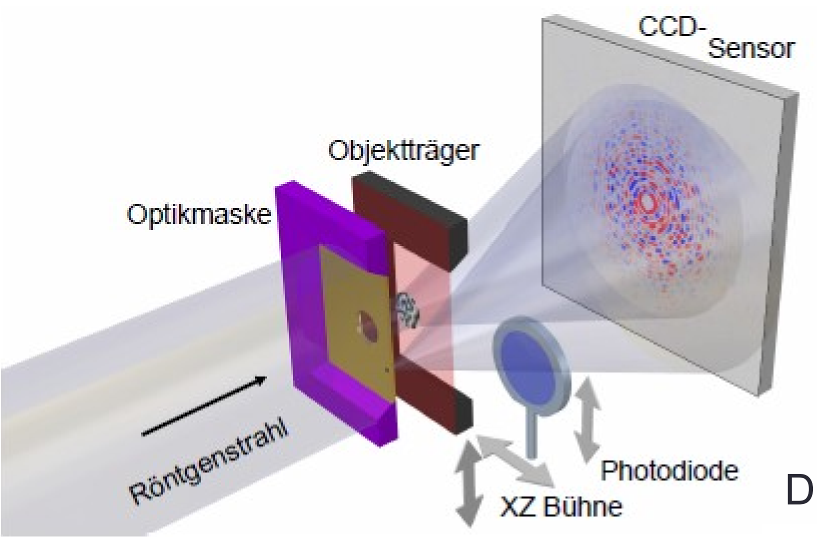

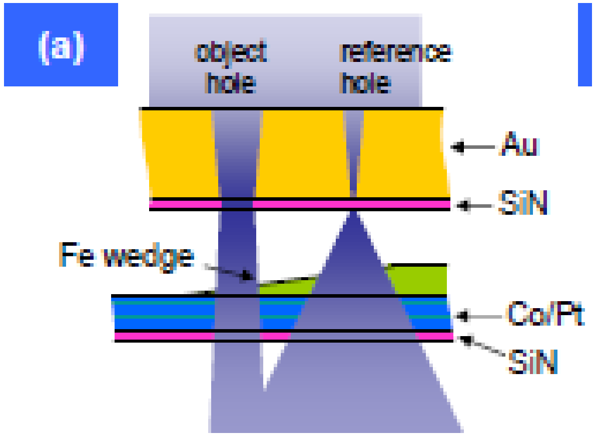

D. Stickler et al., Appl. Phys. Lett. **96**, 042501 (2010)

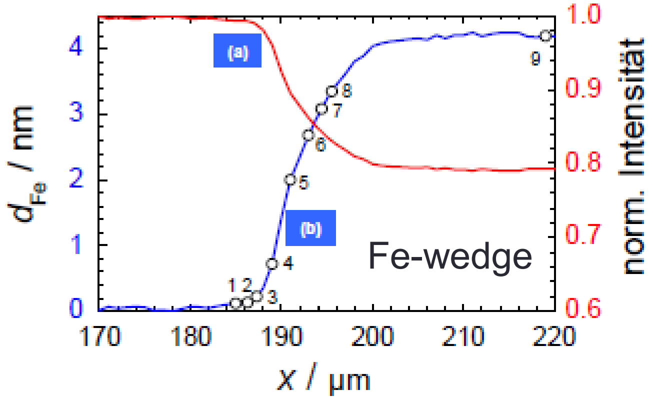

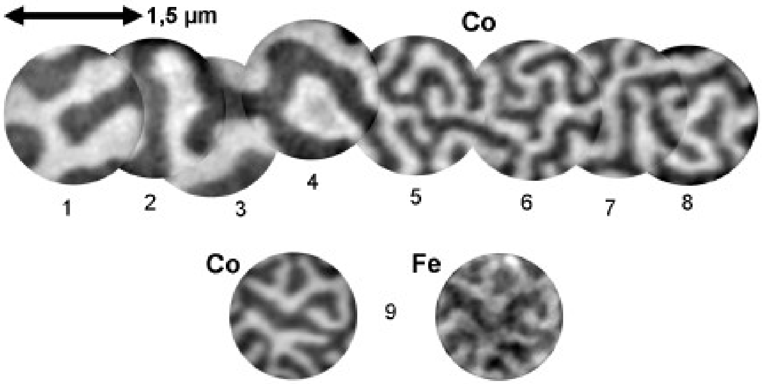

Element-selectivity

XHM – first experimental realization (from Daniel Stickler‘s thesis)

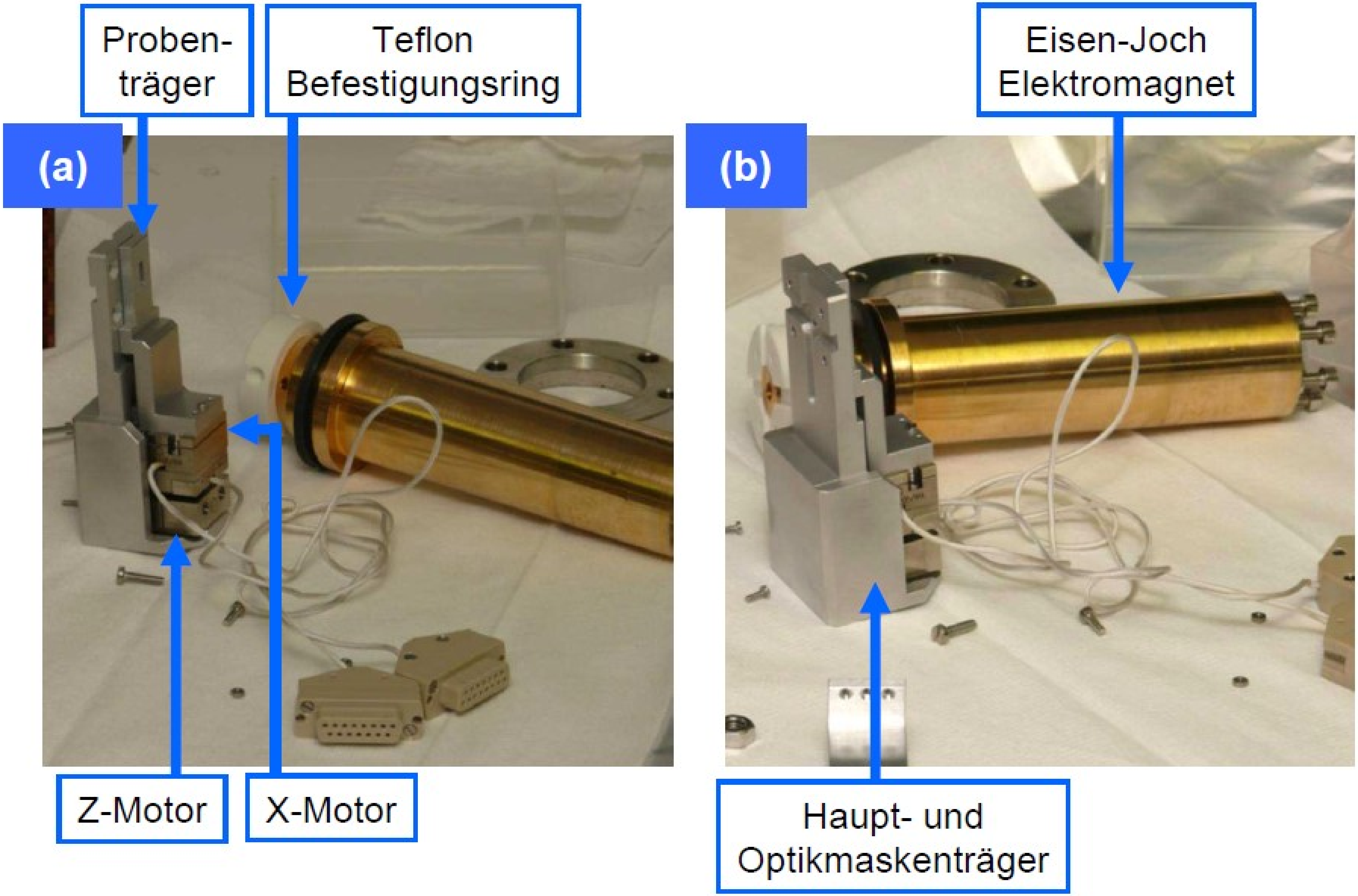

Imaging of magnetic domain patterns with X-rays

> Lensless Imaging – Coherent Diffraction Imaging (CDI)

	Schlüsselelement-Herstellung		Bild-Rekonstruktion	
TXM	Zonenplatte	XXXXX	-direkt-	X
FTH	Optikmaske	XX	Einfache Fourier-Transformation	XX
CDI	-direkt-	X	Phasen-Rückgewinnung	XXXXX